Lagrangian Perspective on the Origins of Denmark Strait Overflow

ATOUSA SABERI, THOMAS W. N. HAINE, AND RENSKE GELDERLOOS

Earth and Planetary Sciences, The Johns Hopkins University, Baltimore, Maryland

M. FEMKE DE JONG

Royal Netherlands Institute for Sea Research, and Utrecht University, Texel, Netherlands

HEATHER FUREY AND AMY BOWER

Woods Hole Oceanographic Institution, Woods Hole, Massachusetts

(Manuscript received 1 September 2019, in final form 16 June 2020)

ABSTRACT

The Denmark Strait Overflow (DSO) is an important contributor to the lower limb of the Atlantic meridional overturning circulation (AMOC). Determining DSO formation and its pathways is not only important for local oceanography but also critical to estimating the state and variability of the AMOC. Despite prior attempts to understand the DSO sources, its upstream pathways and circulation remain uncertain due to short-term (3–5 days) variability. This makes it challenging to study the DSO from observations. Given this complexity, this study maps the upstream pathways and along-pathway changes in its water properties, using Lagrangian backtracking of the DSO sources in a realistic numerical ocean simulation. The Lagrangian pathways confirm that several branches contribute to the DSO from the north such as the East Greenland Current (EGC), the separated EGC (sEGC), and the North Icelandic Jet (NIJ). Moreover, the model results reveal additional pathways from south of Iceland, which supplied over 16% of the DSO annually and over 25% of the DSO during winter of 2008, when the NAO index was positive. The southern contribution is about 34% by the end of March. The southern pathways mark a more direct route from the near-surface subpolar North Atlantic to the North Atlantic Deep Water (NADW), and needs to be explored further, with in situ observations.

1. Introduction

The dense waters entering the Atlantic Ocean from the northern latitudes spill across the Greenland–Iceland–Scotland ridges through two main passages: the Denmark Strait and Faroe Bank Channel. The two overflows merge after entrainment to form the densest constituent of North Atlantic Deep Water (NADW), which is the main contribution to the deep branch of the North Atlantic meridional overturning circulation (AMOC) (Swift et al. 1980; Pratt and Whitehead 2008; Østerhus et al. 2019). The focus of this study is the origins of the dense water that cascades over Denmark Strait, known as Denmark Strait Overflow (DSO). The DSO is a major export route for dense waters in the Nordic Seas, feeding the deep western boundary current (Dickson and Brown 1994). The mean volume transport of the DSO is approximately 3.2 ± 0.5 Sv ($1\,\text{Sv} \equiv 10^6\,\text{m}^3\,\text{s}^{-1}$) (Macrander et al. 2007; Jochumsen et al. 2017). Determining the overflow origins and pathways is important for estimating the state and variability of the AMOC and hence the climate system.

Furthermore, water flowing across a topographic barrier is a ubiquitous process in the ocean and the DSO is a prime example (Pratt and Whitehead 2008). The flows of water through narrow straits, canyons and over topographic features are similar in many ways; these dense overflows undergo significant mixing, entrain ambient fluid, which dilutes the temperature and salinity signal of the water, and increases the volume flow

Denotes content that is immediately available upon publication as open access.

Supplemental information related to this paper is available at the Journals Online website: https://doi.org/10.1175/JPO-D-19-0210.s1.

Corresponding author: Atousa Saberi, atousa.saberi@jhu.edu

DOI: 10.1175/JPO-D-19-0210.1

© 2020 American Meteorological Society. For information regarding reuse of this content and general copyright information, consult the AMS Copyright Policy (www.ametsoc.org/PUBSReuseLicenses).

Downloaded from http://journals.ametsoc.org/jpo/article-pdf/50/8/2393/4989493/jpod190210.pdf by guest on 11 November 2020

(Price and Baringer 1994; Legg 2012). Although the mixing in overflows is highly localized (North et al. 2018), it plays a significant role in influencing the large-scale ocean circulation (Koszalka et al. 2017). Studying the DSO helps us understand common features of climatologically important overflow processes in other parts of the global ocean.

The fate and downstream evolution of the overflow and its variability have been well studied through observations (Macrander et al. 2005; Tanhua et al. 2008) and realistic modeling both in Eulerian (Köhl et al. 2007; Haine et al. 2008; Almansi et al. 2017) and Lagrangian representations of the flow field (Koszalka et al. 2013; von Appen et al. 2014). The formation, sources, and pathways of the DSO have also been studied (Rudels et al. 2002; Köhl et al. 2007). However, despite various proposed circulation schemes based on hydrographic transects (Harden et al. 2016; Våge et al. 2013), the sources and details of the DSO upstream pathways are still uncertain due to mesoscale eddy features, short time scale (3–5 day) variability, mixing, and water mass transformation (Almansi et al. 2017; Spall et al. 2019; Moritz et al. 2019).

There are two main hypothesized sources of the DSO. The first source is the Atlantic-origin water (warmer than 0°C) resulting from transformation in the eastern part of the Nordic Seas (Mauritzen 1996) and the second source is the Arctic-origin water (colder than 0°C) resulting from transformation in the Greenland and Iceland Seas (Swift and Aagaard 1981). The first source is transported primarily by the East Greenland Current (EGC) that flows along the east Greenland shelfbreak. The EGC bifurcates upstream of the Denmark Strait, with one branch continuing along the east Greenland shelfbreak and a separated branch called the separated EGC (sEGC) (Våge et al. 2013) located farther offshore, near the base of the Iceland slope. The contribution of the EGC to the DSO was recognized through hydrography, age analysis, and isotope ratio measurements (Swift et al. 1980; Smethie and Swift 1989; Rudels et al. 2002; Tanhua et al. 2005b).

The second DSO source is carried by the North Icelandic Jet (NIJ), which is centered near the 650 m isobath approaching Denmark Strait from the Iceland slope (Jónsson and Valdimarsson 2004; Våge et al. 2011; Semper et al. 2019). Chemical oceanography studies suggest that there are other water masses contributing to the DSO (Jeansson et al. 2008; Tanhua et al. 2005a), but their percentage of contribution appears to be small (Mastropole et al. 2017). The NIJ and EGC currents are observed to be less distinguishable from each other closer to the Denmark

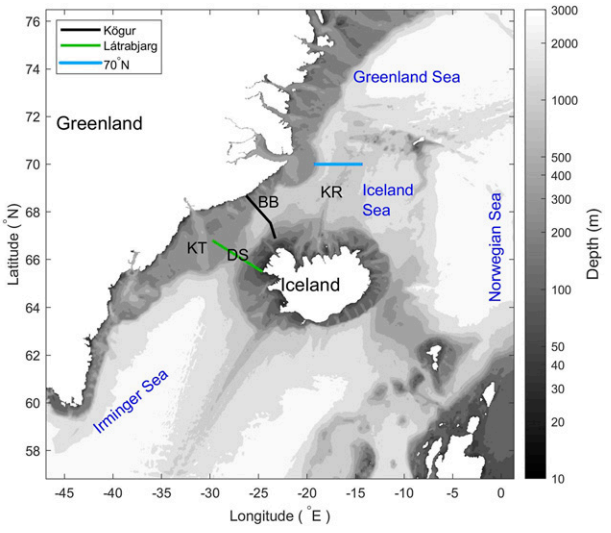

FIG. 1. The bottom topography of the model and model boundaries. The isobath shading is shown in logarithmic intervals. The abbreviation for topographic features are: Denmark Strait (DS), Blosseville Basin (BB), Kolbeinsey Ridge (KR), and Kangerdlugssuaq Trough (KT). The Kögur and Látrabjarg sections are shown with black and green lines, respectively. A section at 70°N, used for comparison with observation is shown with blue line (see Fig. 3). The Nordic seas (the Greenland Sea, Norwegian Sea, and Iceland Sea) and the Irminger Sea are labeled in blue.

Strait (Jónsson and Valdimarsson 2004). To distinguish the currents upstream of Denmark Strait, Harden et al. (2016) analyzed data from a densely instrumented mooring array deployed from September 2011 to July 2012 at the Kögur section, which is roughly 200 km north of Denmark Strait (see Fig. 1). The sEGC is typically found near the base of the Iceland slope and is often difficult to distinguish from the NIJ. In the yearly-mean hydrographic and orthogonal velocity at the Kögur section, the NIJ and sEGC appear as a single feature (Harden et al. 2016). The NIJ also interacts with the (inshore) northward-flowing relatively warm and saline North Icelandic Irminger Current (NIIC) when the bottom topography steers the two currents close together (Pickart et al. 2017).

These studies of the DSO sources and pathways have been mostly based on Eulerian measurements and moorings at historical hydrographic sections. Although they estimate transport and hydrographic properties, they do not conclusively show the connectivity between sections and the evolution of individual currents from one section to another (de Jong et al. 2018). The vertical sections are distant from each other, which makes it challenging to trace the origins of the DSO water through the currents that carry them from one vertical section to the other (Tanhua et al. 2008). There is only one Lagrangian

Downloaded from http://journals.ametsoc.org/jpo/article-pdf/50/8/2393/4989493/jpod190210.pdf by guest on 11 November 2020

study from observations that investigates pathways of dense water using acoustically tracked, high-resolution RAFOS float trajectories (de Jong et al. 2018). These float trajectories revealed new information on the connection between the EGC and the NIJ, and on the subsurface circulation in the Iceland Sea. But they are relatively few in number, and could not be tracked through the Strait itself, leaving some gaps in our knowledge of pathways leading up to the sill (de Jong et al. 2018). Given the complexity of observing pathways leading to the DSO, it is sensible to explore them in a realistic circulation model, in particular to perform backward Lagrangian particle tracking to investigate the origins of the dense waters flowing over the sill at Denmark Strait. Here we apply this technique using a well-studied regional model (Almansi et al. 2017) to trace the near-field origins of the overflow. The available model run, described in detail in the following section, is 15 months long, limiting our ability to study long term trends and seasonality with this particular simulation. Nevertheless, short-term evolution of the Lagrangian particle pathways and hydrographic properties leading up to the sill can be revealed in detail.

The words *origin* and the *DSO* need to be carefully defined. The question of the origin of a water mass is time and space dependent. The farther back in time, the more distributed the *origin* of a water mass in space becomes. It is important to determine how far back in time we are interested in the DSO sources. In this paper, we define the word *origin* as the farthest upstream location from the Denmark Strait in our computational domain within a three month time window, which is the shortest length within the time boundaries of our model run that reveals geographically distinct DSO sources. The DSO needs to be defined as well. In the literature various criteria based on temperature or density have been used (Cooper 1955; Tanhua et al. 2008; Behrens et al. 2017). In this study, we use the most common definition by Dickson and Brown (1994): The DSO is the water with $\sigma_\theta \geq 27.8\,\mathrm{kg\,m^{-3}}$ at the Látrabjarg sill section (see Fig. 1) that flows southward after cascading over the Denmark Strait (by *sill section* we mean the saddle point in the bottom topography that the Látrabjarg section transects). In this paper, we address the following questions: What are the origins and pathways of the DSO? How do the model pathways compare with observed pathways? How do the temperature, salinity, depth and density properties evolve along the DSO pathways? How do the Lagrangian pathways improve our understanding of circulation in the area? How do the main currents interact? What is the best schematic representation of the DSO pathways?

The paper is organized as follows: section 2 presents the details of the numerical model, the particle tracking code, and the observational data used for this study. In section 3 model results are compared with observations, the Lagrangian particle tracking results are presented, and the DSO particle properties, trajectories, and preferred pathways are investigated. A summary and discussion are provided in section 4.

2. Methodology

a. Numerical model configuration

The flow field is calculated using the hydrostatic version of the Massachusetts Institute of Technology General Circulation Model (MITgcm) developed by Marshall et al. (1997). It solves the Navier–Stokes equations under the Boussinesq approximation for an incompressible fluid in a rotating frame of reference. The model domain is configured for the Denmark Strait and it includes the sub-Arctic region from the Greenland Sea to Cape Farewell (Fig. 1). The model simulation period is from 1 September 2007 to 30 November 2008. The temporal resolution of the model is 30 s but the output is stored every 6 h. The horizontal grid resolution is 2 km in the center of the domain from 60° to 71°N (Fig. 1), and it decreases to 4 km moving toward the boundaries. The vertical grid resolution decreases from 2 to 15 m in the upper 120 m and is 15 m thereafter.

The model configuration is identical to that of Almansi et al. (2017), except that the atmospheric forcing at the surface (air temperature, specific humidity, wind, evaporation, precipitation, and radiation) is based on three hourly 15 km resolution fields from the regional Arctic System Reanalysis product (ASRv2; Bromwich et al. 2018). The model is initialized using the global 1/12° reanalysis of the Hybrid Coordinate Ocean Model (HYCOM) + Navy Coupled Ocean Data Assimilation (NCODA) (Cummings and Smedstad 2014), and a coupled ocean–sea ice data assimilation product for the North Atlantic Ocean and Arctic called the TOPAZv4 monthly reanalysis (Sakov et al. 2012). At the open boundaries, time series of velocity, temperature, and salinity from HYCOM + NCODA are used. The sea surface temperature is relaxed to the satellite data from the Operational Sea Surface Temperature and Sea Ice Analysis (OSTIA) global product with a time scale of 5 days (Donlon et al. 2012). The oceanic component is coupled with the MITgcm sea ice model (Losch et al. 2010). Freshwater forcing from runoff, and solid and liquid discharge is used along the Greenland coast from a combination of climate models, remote sensing, and terrestrial data (Noël et al. 2016; Bamber et al. 2012).

Downloaded from http://journals.ametsoc.org/jpo/article-pdf/50/8/2393/4989493/jpod190210.pdf by guest on 11 November 2020

TABLE 1. RAFOS float information, namely, the float ID number, initial pressure (dbar), launch date and position (°N and °W), end date and position, and remarks. The float that was grounded in the Iceland Sea is marked as "ground." The floats that surfaced within the Iceland Sea are marked "IcS." The floats that surfaced within the Labrador Sea are marked "LS." One float surfaced in the Irminger Sea, marked as "IrS."

Float ID	Pres (dbar)	$\text{Date}_{\text{start}}$	$\text{Lat}_{\text{start}}$ (°N)	$\text{Lon}_{\text{start}}$ (°W)	Date_{end}	Lat_{end} (°N)	Lon_{end} (°W)	Remarks
1208	542	12 Jul 2014	70	19	29 May 2015	63.13	54.35	LS
1209	542	12 Jul 2014	70	19	29 May 2015	62.56	58.66	LS
1287	592	13 Jul 2014	69.99	16.76	29 May 2015	66.88	11.95	IcS
1288	572	13 Jul 2014	70	15	29 May 2015	66.88	11.02	IcS
1291	591	13 Jul 2014	69.99	18.62	29 May 2015	66.6	9.52	IcS
1293	595	13 Jul 2014	70	17.01	29 May 2015	66.25	10.93	IcS
1294	579	13 Jul 2014	69.99	17.76	29 May 2015	67.92	15.84	IcS
1297	569	13 Jul 2014	70	18.88	29 May 2015	64.68	34.39	IrS
1298	630	13 Jul 2014	70	18.75	29 May 2015	67.35	23.57	Ground
1301	576	13 Jul 2014	69.99	18.24	29 May 2015	59.80	55.18	LS
1302	593	13 Jul 2014	70	17.25	29 May 2015	67.87	15.21	IcS

b. *Passive Lagrangian particle tracking*

Lagrangian trajectories of virtual particles are calculated using a three-dimensional particle tracking package developed by Koszalka et al. (2013) and Gelderloos et al. (2016) in MATLAB. For this study, the code is extended to compute the trajectories at a single depth level in isobaric mode as well. The algorithm employs a MATLAB built-in ordinary differential equation (ODE) solver to solve for particle position at each time step. The particles at each time step are advanced with the two- or three-dimensional velocity field linearly interpolated to the instantaneous position of the particle. The code does not have explicit diffusion, as we assume all the information about the flow is contained in the velocity field output of the MITgcm model. The velocity component normal to boundaries is zero and the particles slide along the solid boundaries of the domain. The evolution of tracer fields such as salinity and temperature along the Lagrangian paths are obtained by nearest-neighbor interpolation of the model output to the particle positions. The model equation of state (Jackett and McDougall 1995) is then used to compute the density of the particles.

c. *Observations*

Several observational datasets are compared to the model output to build confidence in the realism of the model. Shipboard data, moorings, and hydrographic sections are used to perform the comparison in an Eulerian frame, while RAFOS float trajectories and properties (de Jong et al. 2018) are used to perform the comparison in a Lagrangian frame.

1) KÖGUR MOORING ARRAY

To perform model–data comparison upstream of Denmark Strait, data from the Kögur mooring array is used. Harden et al. (2016) analyzed results from a year-long densely instrumented mooring array upstream of the Denmark Strait, across the Blosseville Basin and along the Kögur section (shown in Fig. 1). Each of the 12 moorings was equipped with instruments measuring temperature, salinity, pressure, and current velocity. The data coverage is from 29 August 2011 to 30 July 2012. The hydrographic and the velocity data are interpolated into a structured grid with a spatial resolution of 8 km in the horizontal and 50 m in the vertical direction. The temporal resolution of the gridded product is 8 h. Harden et al. (2016) explain the details of the data and interpolation scheme used for gridding the data in their appendixes A and B.

2) RAFOS FLOAT AND SHIPBOARD DATA

To make a direct comparison between the model Lagrangian trajectories and the floats, we use isobaric RAFOS floats deployed near 70°N on a zonal section in July 2014 (de Jong et al. 2018). The complete RAFOS dataset contained 52 floats, but only the 11 floats that drifted near the Denmark Strait are considered here. The information about these floats studied here is listed in Table 1. They are isobaric subsurface drifters ballasted for the depth of interest and the hydrographic properties of the study region (Rossby et al. 1986). The floats were tracked by acoustic signals on a daily schedule from six sound sources moored in the Iceland Sea (de Jong et al. 2018). They provide pressure, temperature, and arrival times of acoustic signals along their trajectories. They were deployed in water with $\sigma_\theta > 28.0\,\text{kg}\,\text{m}^{-3}$ in order to be embedded in the overflow water. At the RAFOS float deployment locations, shipboard conductivity–temperature–depth (CTD) measurements were taken. The CTD data are used to make a direct comparison of temperature and salinity at the initial positions of the RAFOS floats and the modeled Lagrangian particles.

Downloaded from http://journals.ametsoc.org/jpo/article-pdf/50/8/2393/4989493/jpod190210.pdf by guest on 11 November 2020

3) HYDROGRAPHIC DATA

Data provided by the Marine and Freshwater Research Institute (Malmberg and Valdimarsson 2003) are used to verify the realism of the model at the Látrabjarg section. The data are from a monitoring project in Icelandic waters that has been ongoing since 1990 (Malmberg and Valdimarsson 2003), and the research on the Icelandic waters hydrographic variability and environmental effects on Icelandic fisheries (Palsson et al. 2012). In addition, hydrographic profiles from the years 1980 to 2017 on the Iceland shelf are collected from various databases such as Unified Database for Arctic and Subarctic Hydrography (Behrendt et al. 2017), World Ocean Database (NOAA 2013), and International Council for the Exploration of the Seas (ICES 2006). These data are used to better understand the characteristics of water on the Iceland shelf.

3. Results

a. Comparison with observations

1) MOORINGS AT KÖGUR

The model results are compared with the year-long mean hydrographic properties and orthogonal velocity from the Harden et al. (2016) Kögur mooring deployment (Fig. 2). Although the year of observation (2011–12) does not coincide with the modeled year (2007–08), the hydrographic structures from the model (Figs. 2a,c) match the observations (Figs. 2b,d) well. The transition from warm and salty North Atlantic water with subtropical origin (referred to as Irminger Water) to the cold and fresh Polar Surface Water in the upper layer is evident in both the model and observations along the section from east to west. The cold and fresh Polar Surface Water extends across the section from the west in both cases. The Irminger Water region extends somewhat further in the observations than in the model.

Harden et al. (2016) observed two water masses below the 27.8 kg m^{-3} isopycnal: the Recirculated Atlantic Water and Arctic-origin Water. The Recirculated Atlantic Water, defined by potential temperature $\theta > 0$°C and salinity $S > 34.9$, is observed between depths of 300 and 800 m. The Arctic-origin Water with $\theta < 0$°C and $\sigma_\theta > 28$ kg m^{-3} is found below 800 m closer to Greenland, but it can also be seen at shallower depths on the Iceland slope. These two water masses can be seen in the model, too; however, the model mean potential temperature is higher by about 0.2°C in the deeper part of the section (below 1200 m), and also the Arctic-origin Water is less extended to the Iceland side of the Strait.

The isopycnal structure in the model is similar to that of the observations in the middle and western parts of the section. However, the slope of isopycnals is steeper toward the Iceland shelf in the observations, which has dynamical implications for the strength of the NIJ. The model has a lower shear and slightly smaller orthogonal velocity in the year-long mean field as shown in Figs. 2e and 2f. The individual snapshots (not shown) have better consistency with observations in isopycnal structure. Moreover, the isopycnals are slightly deeper in the model, consistent with the deep warm bias found at Denmark Strait by Almansi et al. (2017).

The orthogonal velocity in both Figs. 2e and 2f consists of two main equatorward currents, one on the Greenland side and the other on the Iceland side. The model agrees well with the observations in capturing the surface-intensified East Greenland Current on the Greenland shelf break. The EGC maximum velocity at its core is 0.3 m s^{-1} in both model and observations. As Harden et al. (2016) describe, on the Iceland side there are two distinct currents that appear as a single feature in the mean field: the NIJ, a middepth intensified flow positioned near the 650 m isobath, and the sEGC, a surface-intensified current located seaward of the NIJ. In the annual mean field, the NIJ and the sEGC have one core in both observations and model. However, the two currents appear as distinct features with separated cores in some individual snapshots (not shown). Using orthogonal velocity to distinguish the two currents can be difficult due to the transient nature of the NIJ and sEGC. Below, the Lagrangian particles help us understand the pathways and variability of the two currents.

Besides the equatorward currents, there are two regions with mean poleward velocity. One is the NIIC on the Iceland shelf that carries warm subtropical-origin water into the Nordic Seas. The other is a weak flow on the Iceland slope that Harden et al. (2016) attributed to a signature of recirculation of water that previously passed through the section. The model orthogonal velocities are consistent with these observations (Figs. 2e,f), and the model Lagrangian particle trajectories confirm the recirculation (see section 3b below).

2) COMPARISON WITH FLOAT AND SHIP DATA

Figure 3 shows a comparison between data from the shipboard CTD survey on the release date of the RAFOS floats with the model results. The CTD survey took place in July 2014. As the observations comprise a single snapshot in time, in order for the comparison to be relevant, the mean potential temperature and salinity in the month of July from the model is used. The CTD data is also compared with daily snapshots in the month of

Downloaded from http://journals.ametsoc.org/jpo/article-pdf/50/8/2393/4989493/jpod190210.pdf by guest on 11 November 2020

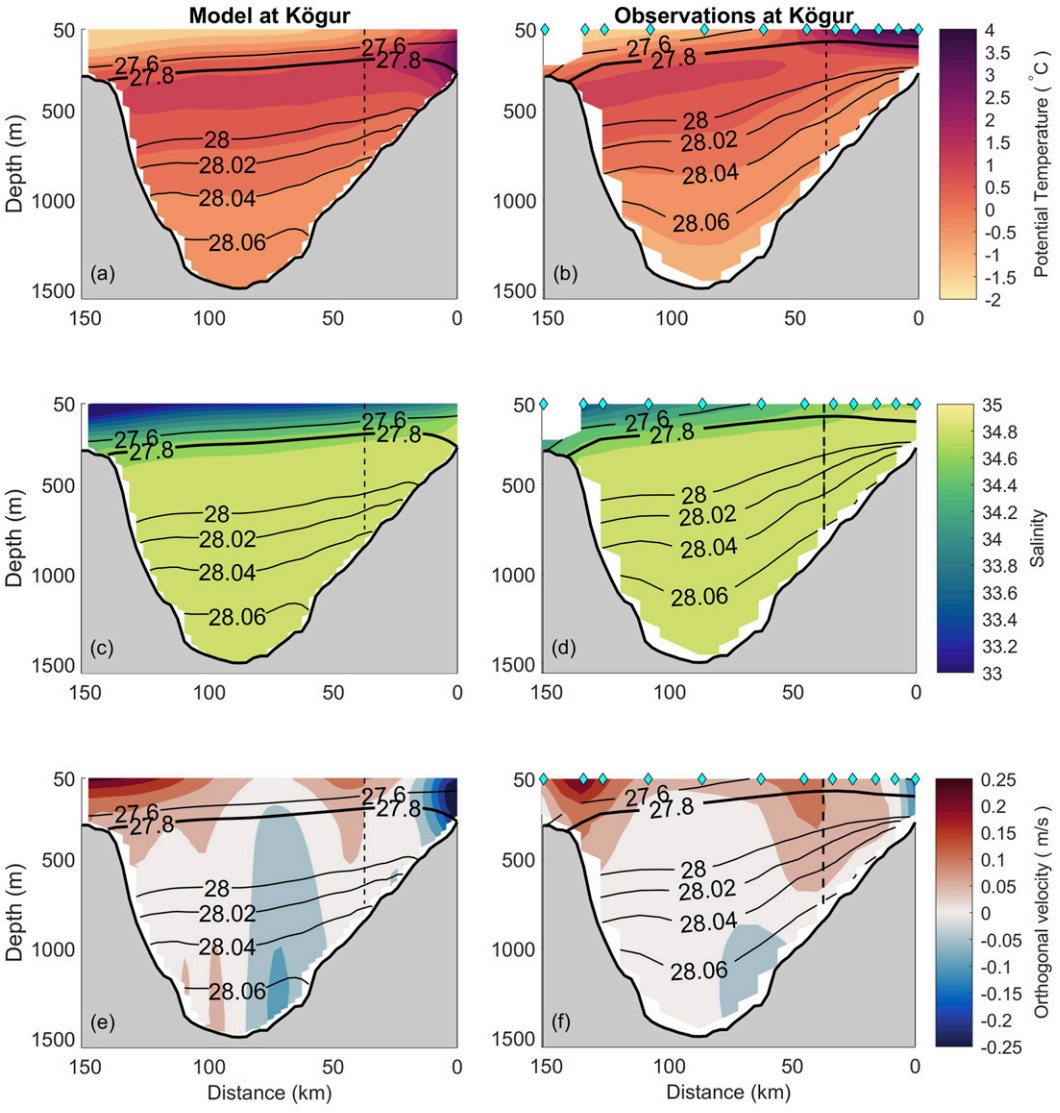

FIG. 2. Comparison of year-long mean hydrographic properties and orthogonal velocity (a),(c),(e) from the model and (b),(d),(f) with mooring observations at the Kögur section. Distance is measured along the section from the Iceland shelf break. The mooring locations are marked by cyan diamonds. Isopycnals are contoured in black. The 27.8 kg m^{-3} isopycnal is highlighted by the bold black contour. The vertical dashed line indicates the location where the orientation of the section changes (see Fig. 1). The equatorward orthogonal velocities in (e) and (f) are positive.

July from the model (not shown), and no significant difference with the mean section was observed. The depth and overall structure of the isopycnals in the model are similar to the observations. The deepening and shoaling of 28.05 kg m^{-3} isopycnal varies in daily snapshots, but the average depth of the isopycnal is consistent with the observations. The surface temperature along the section is also consistent. East of 17°W the water column temperature and salinity structure are in good agreement with the data, but the model is slightly fresher. However, the subsurface temperature and salinity near the Greenland shelf from 50 to 380 m depth is higher by 1.15 ± 0.77°C and 0.4 ± 0.27 in the observations. Between 380 and 750 m, which includes the depth range where the floats are released, the model agrees well with the observations.

To determine how the hydrographic properties evolve in time, we also compare the model with observations in a Lagrangian framework. A set of 400 particles seeded at 70°N are tracked forward in time in isobaric mode at 600 m depth. This mimics the constraint placed on the RAFOS float trajectories listed in Table 1. The depth of

Downloaded from http://journals.ametsoc.org/jpo/article-pdf/50/8/2393/4989493/jpod190210.pdf by guest on 11 November 2020

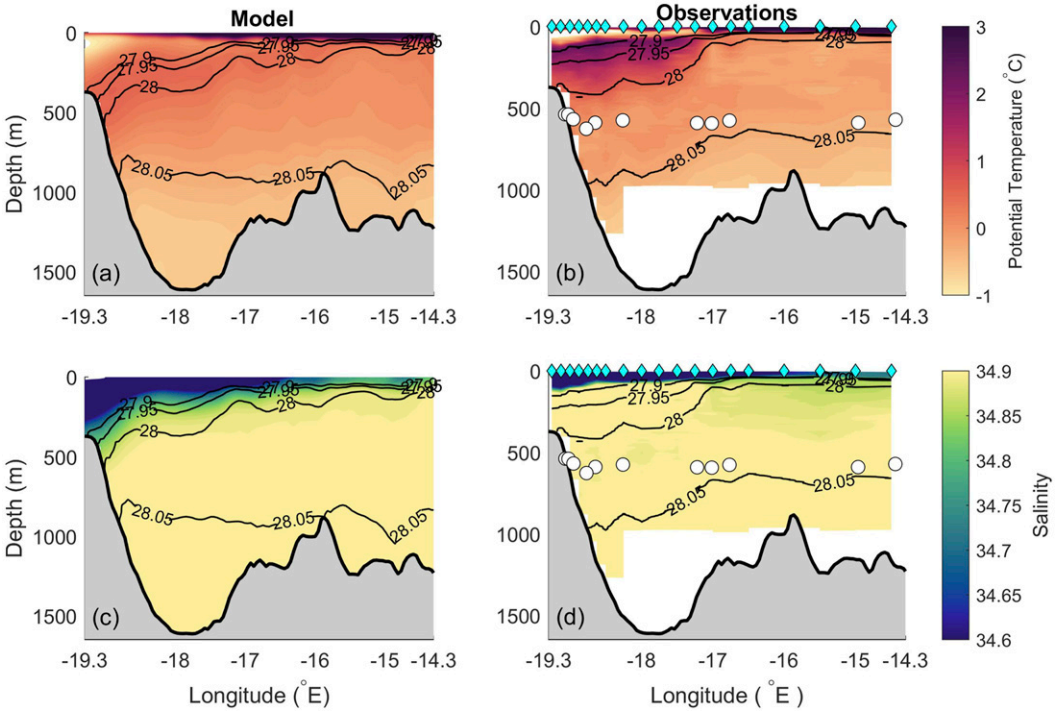

FIG. 3. Comparison of hydrographic properties at 70°N from (a),(c) the model with (b),(d) CTD sections surveyed in July 2014 at the RAFOS float release date. The model vertical section is the mean of July 2008. The station positions along the section are marked by cyan diamonds. Isopycnals are shown with black contours. The release position along the section and depth of the RAFOS floats considered in this study are marked by white circles. Note that all of the floats are located deeper than 500 m.

600 m is used because it is close to the average depth of the floats (560 m). Figure 4 shows the float trajectories and simulated Lagrangian particle trajectories and the evolution of temperature and pressure along these paths. The RAFOS trajectories are compared with the modeled particle trajectories for 139 days during the same time of the year from mid-July to the end of November, which was the last day at which the model outputs are available.

The observed float trajectories are within the range of the modeled particle trajectories. The EGC is visible in both the observed and modeled particle trajectories. The model particles also reveal a northward flow offshore of the EGC. This pathway is due to intermittent eddies visible in the Eulerian velocity field at 600 m depth, which was not likely to be captured by only the two floats released close to it. In Figs. 4a and 4b, the evolution of temperature and pressure for the 11 selected floats are shown. The ∅(100) m spikes in one float's (RFS1209) pressure record occurred when that float was traveling along the east slope of Greenland, embedded in the EGC (Fig. 4b). These pressure excursions are coincident with the float measuring warmer temperatures (~0.5°C warmer, Fig. 4a), and were likely due to the float being pushed upslope by strong upwelling. Evidence of upslope excursions, measured by other floats included in the complete RAFOS dataset, were found in other locations in the Iceland Sea, and most prevalent along the northwest slope of Iceland (de Jong et al. 2018). Some of the float temperature measurements fall within the envelope of model particle temperatures. However, some others are colder than model particles by 0.1 ± 0.045°C, which is well within the range of observed interannual variability (Lauvset et al. 2018). The RAFOS floats were not equipped with conductivity sensors; therefore, salinity evolution along the float trajectories is not possible.

3) COMPARISON AT THE LÁTRABJARG SECTION AND EVIDENCE OF DENSE WATER ON THE ICELAND SHELF

The fidelity of the model has already been studied at the Látrabjarg section by Almansi et al. (2017), who showed that the model hydrography resembles shipboard CTD observations between 1990 and 2012 at Látrabjarg (Fig. 4 in Almansi et al. 2017). That study concluded that the model captures all of the major currents (the NIIC, the NIJ, and the EGC) along the

Downloaded from http://journals.ametsoc.org/jpo/article-pdf/50/8/2393/4989493/jpod190210.pdf by guest on 11 November 2020

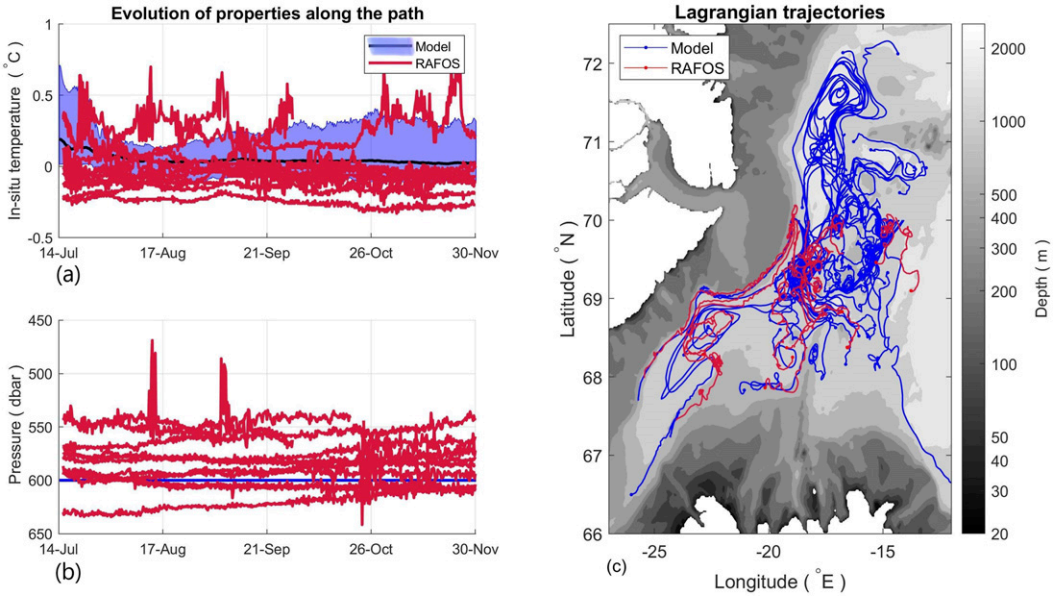

FIG. 4. Evolution of (a) in situ temperature and (b) pressure of model Lagrangian particles and RAFOS floats. The blue shade shows the 5th and 95th percentile ranges of the particle temperatures. The solid black line shows the mean particle temperature. The red lines show the RAFOS float time series. All the modeled particles are confined to 600 m depth [the blue line in (b)]. (c) Lagrangian trajectories of the model particles (blue) and the RAFOS floats (red). Only 50 model trajectories are shown.

section. The hydrographic structures are shown to be consistent with the detailed observational studies performed by Mastropole et al. (2017) at Denmark Strait. The comparison by Almansi et al. (2017) was focused on the western side of the Denmark Strait where the bottom intensified DSO is located. The DSO is the dense ($\sigma_\theta \geq 27.8\,\mathrm{kg\,m^{-3}}$) southward flow banked against the Greenland side of the trough in Denmark Strait. However, observations show evidence for the existence of dense water (satisfying the DSO density criterion) on the Iceland shelf occasionally in winter (Våge et al. 2015). In Fig. 5 the model-mean section in February is compared with observations from February 1997. They both show steep isopycnals from 27.6 to $27.8\,\mathrm{kg\,m^{-3}}$ on the Iceland shelf. The $27.8\,\mathrm{kg\,m^{-3}}$ isopycnal on the Iceland shelf lies farther westward in the model than the observations by approximately 70 km, and it continues through the trough and changes slope on the Greenland side. The same isopycnal structure is evident from the observations but for the 27.6 and $27.7\,\mathrm{kg\,m^{-3}}$ isopycnals. The continuity of isopycnals from the Iceland shelf to the trough is seen from January to March in the model with the isopycnals being steep and outcropping to the surface by the end of February and early March. The model shows biases in the surface salinity (about +0.1 or less), which could be the potential reason why the dense water at the shelf appears to occupy a larger area than the observations. The dense water on the Iceland shelf has been observed in other years as well; however, it is sparse in winter. Our exploration of the Unified Database for Arctic and Subarctic Hydrography (Behrendt et al. 2017), World Ocean Database (WOD 2013), and International Council for the Exploration of the Seas (ICES 2006) database revealed that out of 3700 individual profiles near the Iceland shelf (within about 100 km periphery of Iceland's west coast) spanning from 1980 to 2018, about 800 of them were collected in the winter (JFM). Despite the limited winter observations, 20 out of 200 profiles show the dense water ($\sigma_\theta \geq 27.8\,\mathrm{kg\,m^{-3}}$) on the shelf along Látrabjarg section (in depths shallower than 230 m). These 20 profiles are spread over the years 1981–84, 1990, 1993, and 1995, which have relatively high North Atlantic Oscillation (NAO) index.

b. *Backward tracking of particles released at Látrabjarg*

To determine the near-field origins and pathways of the DSO, passive particles are released at the Látrabjarg section at the end of each month from 30 November 2007 to 31 October 2008. There is an ensemble of 12 particle release experiments (see Table 2). Each ensemble member is tracked backward in time for 3 months in three-dimensional space. This length of time was chosen because it is the shortest time period at which the geographical distribution of pathways, the water masses and properties of the DSO sources

Downloaded from http://journals.ametsoc.org/jpo/article-pdf/50/8/2393/4989493/jpod190210.pdf by guest on 11 November 2020

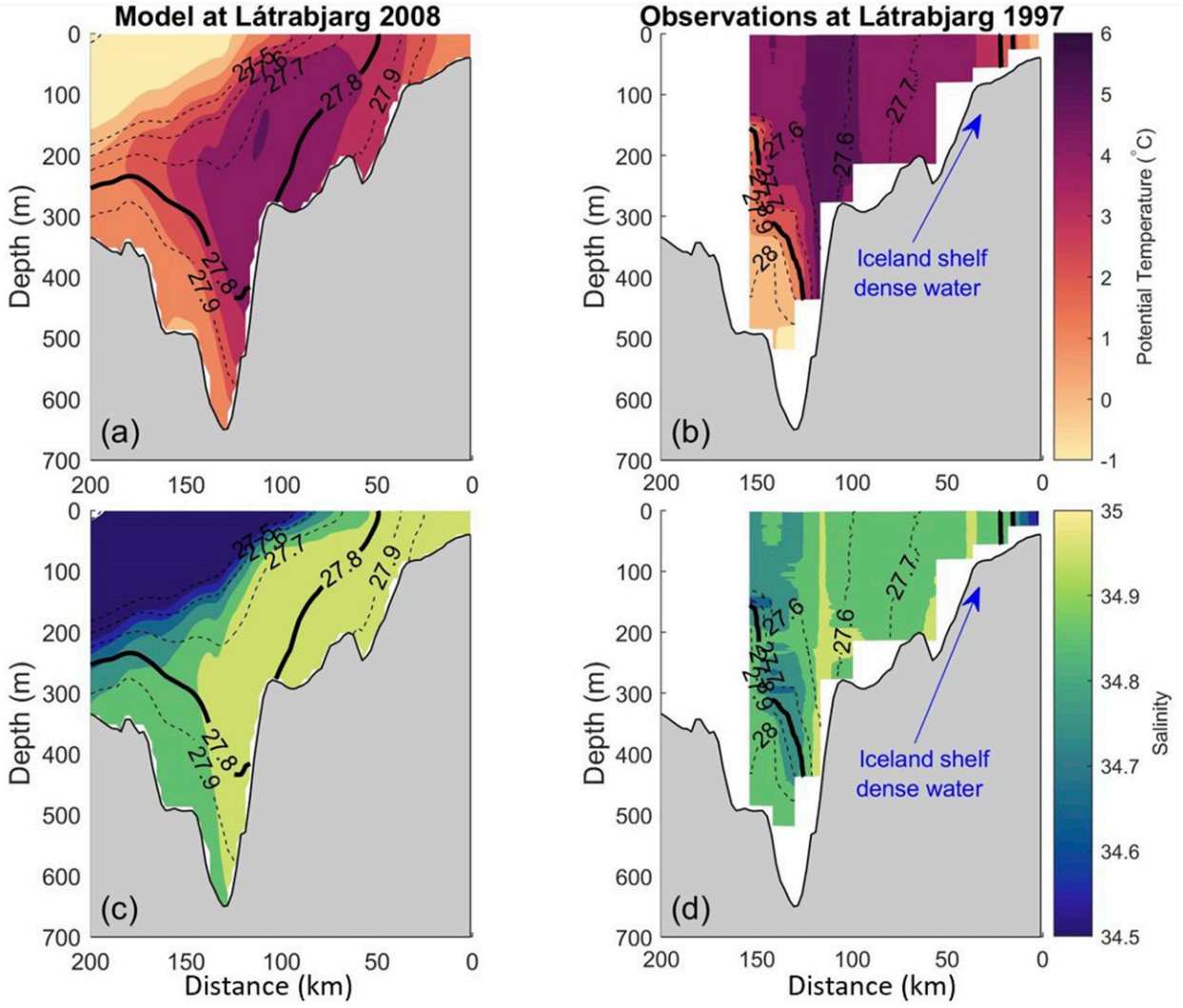

FIG. 5. Comparison of hydrographic properties from (a),(c) the model with (b),(d) CTD sections surveyed in February 1997 at the Látrabjarg section (see Fig. 1). The model vertical section is the mean of February 2008. The February 1997 is selected as the observational evidence for the dense water on the Iceland shelf. Isopycnals are contoured in black. The 27.8 kg m^{-3} isopycnal is highlighted by the bold black contour. The Iceland shelf dense water in the observations is annotated by the arrows.

can be identified. We explored backtracking of longer time period (4, 5, and 6 months) to be sure 3 months was an appropriate time scale. The particle seeding resolution is 0.5 km in the horizontal and 25 m in the vertical direction. All particles are seeded below the 27.8 isopycnal satisfying the conventional overflow threshold in the literature, which we refer to as dense particles (see Table 2). The total number of backward tracked dense particles over all ensemble members is 18 399.

The backward tracking alone does not reveal what fraction of the dense water eventually cascades over Denmark Strait. Therefore, each ensemble member is also advanced forwards for 30 days. Particles that appear south of Denmark Strait after 30 days are considered to have participated in the DSO, regardless of their final density. The total number of these so-called DSO particles is 13 708, which is 74.5% of all the dense particles. It is found that the ratio of the DSO to the dense particles varies between ensemble members. The information about each ensemble member is listed in Table 2. Notice that although the number of dense particles is highest in February and March, the number of DSO particles does not increase proportionally. In fact, the ratio of the DSO to the dense particles decreases in March. This is because the Irminger Current is colder in winter and spring (by 1.8°C; Mastropole et al. 2017), and becomes denser as it moves northward until some of it

Downloaded from http://journals.ametsoc.org/jpo/article-pdf/50/8/2393/4989493/jpod190210.pdf by guest on 11 November 2020

TABLE 2. Particle information, namely, the release ID, release date at Látrabjarg section, date at 90 days prior to reaching the Látrabjarg section (date at the origin), date 30 days after passing the Látrabjarg section (date at the end), the number of particles that have $\sigma_\theta \geq 27.8\,\mathrm{kg\,m^{-3}}$ (dense particles), and the number of particles that eventually end up south of the Denmark Strait (DSO particles).

Release ID	Release date at Látrabjarg	Date at the origin	Date at the end	No. of dense particles	No. of DSO particles
I	30 Nov 2007	1 Sep 2007	30 Dec 2007	514	466
II	31 Dec 2007	2 Oct 2007	30 Jan 2008	856	773
III	31 Jan 2008	2 Nov 2007	1 Mar 2008	1800	1041
IV	29 Feb 2008	1 Dec 2007	30 Mar 2008	2442	1694
V	31 Mar 2008	1 Jan 2008	30 Apr 2008	2024	1006
VI	30 Apr 2008	31 Jan 2008	30 May 2008	1852	1225
VII	31 May 2008	2 Mar 2008	30 Jun 2008	1508	1120
VIII	30 Jun 2008	1 Apr 2008	30 Jul 2008	1341	1153
IX	31 Jul 2008	2 May 2008	30 Aug 2008	1791	1427
X	31 Aug 2008	2 Jun 2008	30 Sep 2008	1647	1380
XI	30 Sep 2008	2 Jul 2008	30 Oct 2008	1726	1612
XII	31 Oct 2008	2 Aug 2008	30 Nov 2008	898	811

satisfies the $\sigma_\theta \geq 27.8\,\mathrm{kg\,m^{-3}}$ criterion. This dense water continues northward and mixes with surrounding water, namely, the southward flowing EGC and NIJ, and some fraction of it cascades over Denmark Strait within 30 days. This splitting and retroflection of the Irminger Current in the vicinity of the Denmark Strait was demonstrated by Valdimarsson and Malmberg (1999) and discussed in Rudels et al. (2002) as well. However, in that study, the location of the splitting was not fully identified. The Lagrangian trajectories in the following section reveal the time-varying location of this bifurcation. For the rest of the paper, the DSO particle trajectories and hydrographic properties are discussed; studying the properties and pathways of dense water that does not cascade over the Denmark Strait (the difference between columns 5 and 6 in Table 2) is beyond the scope of this research.

The backward trajectories of the DSO particles reveal different sources for the DSO. Figure 6a shows the geographical distribution of the particles three months before reaching the Látrabjarg section, at their origin, color coded by ensemble member (see also Table 2). The DSO particles come from both north and south of the Denmark Strait, with 83.6% originating from the north. The geographical distribution of the DSO particles at their origins are nearly identical throughout the year between all ensemble members, but the fractions from north and south of the sill vary. To study this variability for each ensemble member, the DSO particles are categorized into different subsets, based on geographical origin. They are naturally broken down into the northern- and southern-origin subsets. The southern origin subset is further separated into two groups, depending on whether they arrive at the Icelandic side of the Látrabjarg section east or west of 26.5°W (star marker on Fig. 6a). Figure 6b shows the variation in the fraction of the DSO particles flowing from the north (abbreviated as N), the south and west of 26.5°W (abbreviated as S), and the south and east of 26.5°W, on the Iceland shelf (abbreviated as ISh) for each ensemble member. In summary, the DSO particles are categorized into N, S, and ISh subsets based on where they originate. The trajectories and properties of the particles in each individual subset are now discussed in detail.

The fraction of the DSO particles from the south (S + ISh), which is persistent throughout the year, is highest at the end of March (ensemble member V), with a mean contribution of 16.3%. The contribution from the ISh subset is present only between 31 December to 30 April (ensemble members III, IV, V, and VI) with a peak of 12.8% of DSO particles at the end of February. The depth–longitude positions of the DSO particles at the Látrabjarg section can be seen in Fig. 7, color coded by the origin subsets. Note that the S and N subsets both occupy the western side of the section and the ISh subset, separated from the others, occupies the eastern side of the section. The presence of DSO particles in depth–longitude space is consistent with the observations of dense water at the Látrabjarg section, discussed earlier (Fig. 5).

The DSO particles are tracked backward from their release point at the Látrabjarg section. However, for the sake of visualization, analysis, and discussion their trajectories are plotted forward in time to the Látrabjarg section. Figure 8 shows the trajectories of the DSO particles approaching Denmark Strait. To avoid clutter, instead of plotting the full trajectories of individual particles, 10-day-long pathlines of every 5th DSO particle in each subset are plotted. The visualized trajectories are representative of trajectories of all the DSO particles. Note that, not all the DSO particle trajectories at all times look like the trajectories in Fig. 8 (see the supplemental animations). The northern pathway (in blue) is present in all months. The DSO particle

Downloaded from http://journals.ametsoc.org/jpo/article-pdf/50/8/2393/4989493/jpod190210.pdf by guest on 11 November 2020

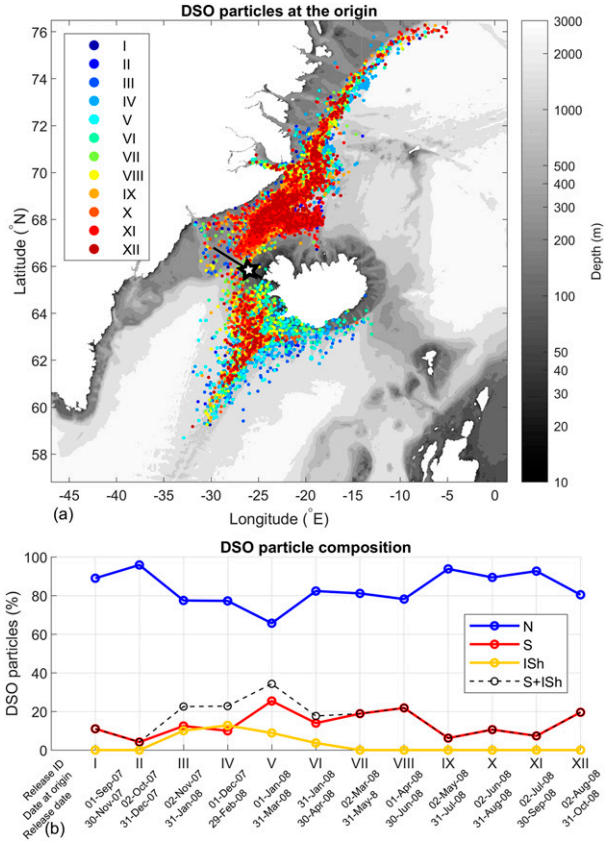

FIG. 6. (a) The geographical distribution of the DSO particles at their origins color coded by ensemble member ID. (b) The fractions of the DSO particles in each subset. The fractions are variable for each ensemble member. N, S, and ISh in the legend mark the north (blue), the south and west of 26.5°W (red) and the south and east of 26.5°W on the Iceland shelf (yellow) subsets, respectively (see Fig. 15 for the subsets). The 26.5°W is marked with the star. The dates at the origin and the release dates at Látrabjarg are shown below the abscissa. The total contribution from the south is highest for release V.

trajectories in subset N depict the conventional route of the DSO along the east Greenland shelf break; that is, the EGC. The bifurcation of the EGC is also evident from the trajectories (and better visualized in the animations): sometimes the separation takes place north of the Kögur section (≈68°N in ensemble members I, IV, VI, and IX), and other times the separation takes place south of it within the southern part of the Blosseville Basin (≈67°N in ensemble members V and VIII). The particle trajectories show that the separation from the EGC takes place in multiple locations along the east Greenland shelf (mostly south of ≈70°N). The trajectories of DSO particles in the N subset show that sometimes the bifurcated branches reunite with the EGC (e.g., in ensemble members III and IX), and other times they shift to the middle of the basin and continue south. Concurrently, the NIJ is evident from the Lagrangian particle trajectories on the northwest Iceland slope: sometimes very close to the Kolbeinsey Ridge (e.g., in ensemble members I, IV, X, XI, and XI) and sometimes about 130 km southwest of the ridge, closer to the Kögur section (e.g., in ensemble members V–VII). The DSO particle trajectories also reveal that sometimes the sEGC swings toward the Iceland shelf, interacts with the NIJ and the two currents merge and continue south along the Iceland shelf. This interaction is clearly visible from the animations of particle trajectories, provided as supplemental material. Notice that, although the particles follow the currents, they do not necessarily stay in one current at all times. In other words, the Lagrangian trajectories are in principle distinct from the currents (velocity maxima). The separation from the EGC and its interaction with the NIJ is also observed by Våge et al. (2013). The interaction happens at different times and places along the path for each ensemble member. As the simulated trajectories cover only one year, detecting the sEGC and the separation frequency is hard; nevertheless, there is no strong evidence of seasonality. Besides, as discussed above, the sEGC appears to be intermittent.

The DSO particles in the S and ISh subsets have a similar spatial distribution at their origins for ensemble members III–VI (Fig. 8). The majority of particles in the ISh subsets, however, move along shallower isobaths (depth ≤ 300 m, Fig. 12c) than the particles in the S subsets (depth ≈ 400–800 m, Fig. 11c). Particles in both subsets flow northward toward the Denmark Strait. The particles in the S subset then encounter the southward flowing particles in the N subset, retroflect, and flow south again, to reach the western side of the Látrabjarg section. In contrast, the northward flowing ISh particles arrive at the eastern side of the Látrabjarg section and predominantly continue northward with the NIIC. Most of these particles return south within 20 days of crossing the Látrabjarg section in the forward run. Figure 9 shows the particle trajectories at the end of the forward run for each ensemble member. The particles in the S and N subsets cascade over Denmark Strait and trace multiple recirculations in the Kangerdlugssuaq Trough. These cyclonic recirculations are also detected by Koszalka et al. (2013). Finally, the recirculated particles continue to flow south along the east Greenland shelf following the traditional DSO path (Dickson and Brown 1994). Similarly, the particles in the ISh subsets cascade over Denmark Strait but with a time lag of about 20 days compared to the other subsets. They then follow a similar path to the particles from the N and S subsets. Notice that very close to the Látrabjarg section immediately before and after cascading the Denmark Strait, the particles

Downloaded from http://journals.ametsoc.org/jpo/article-pdf/50/8/2393/4989493/jpod190210.pdf by guest on 11 November 2020

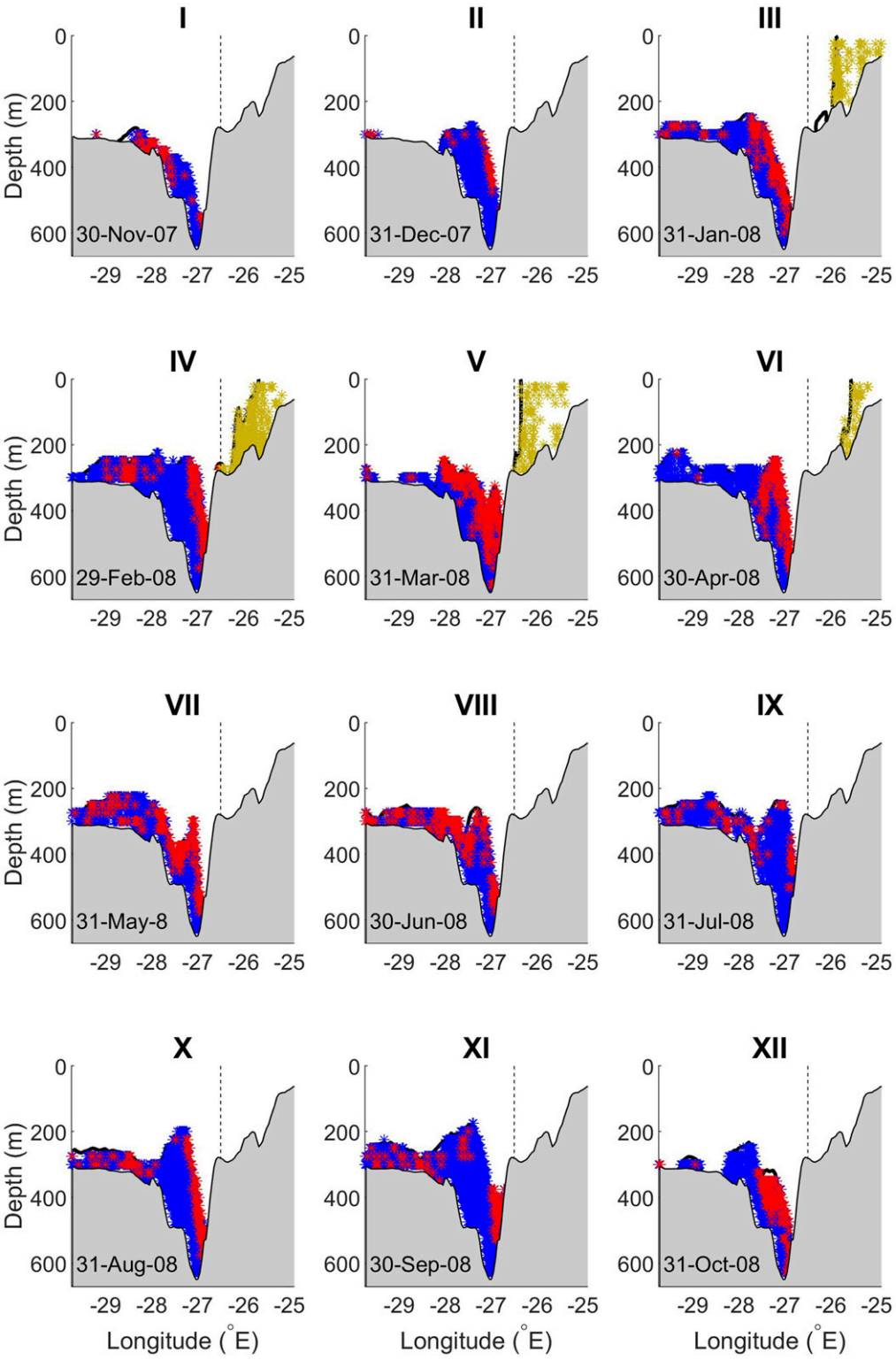

FIG. 7. Depth–longitude distribution of the DSO particles at the Látrabjarg section. The particles are color coded by the origin subsets for each ensemble member as in Fig. 6b (particle trajectories in N, S, and ISh subsets are colored in blue, red, and yellow). For clarity, the release dates of particles at the Látrabjarg section are shown (also see Table 2). The 27.8 kg m^{-3} isopycnal is highlighted by the bold black contour. The vertical dashed lines at 26.5°W separate the ISh subsets from the rest of the south particles (the S subsets) for each ensemble member.

Downloaded from http://journals.ametsoc.org/jpo/article-pdf/50/8/2393/4989493/jpod190210.pdf by guest on 11 November 2020

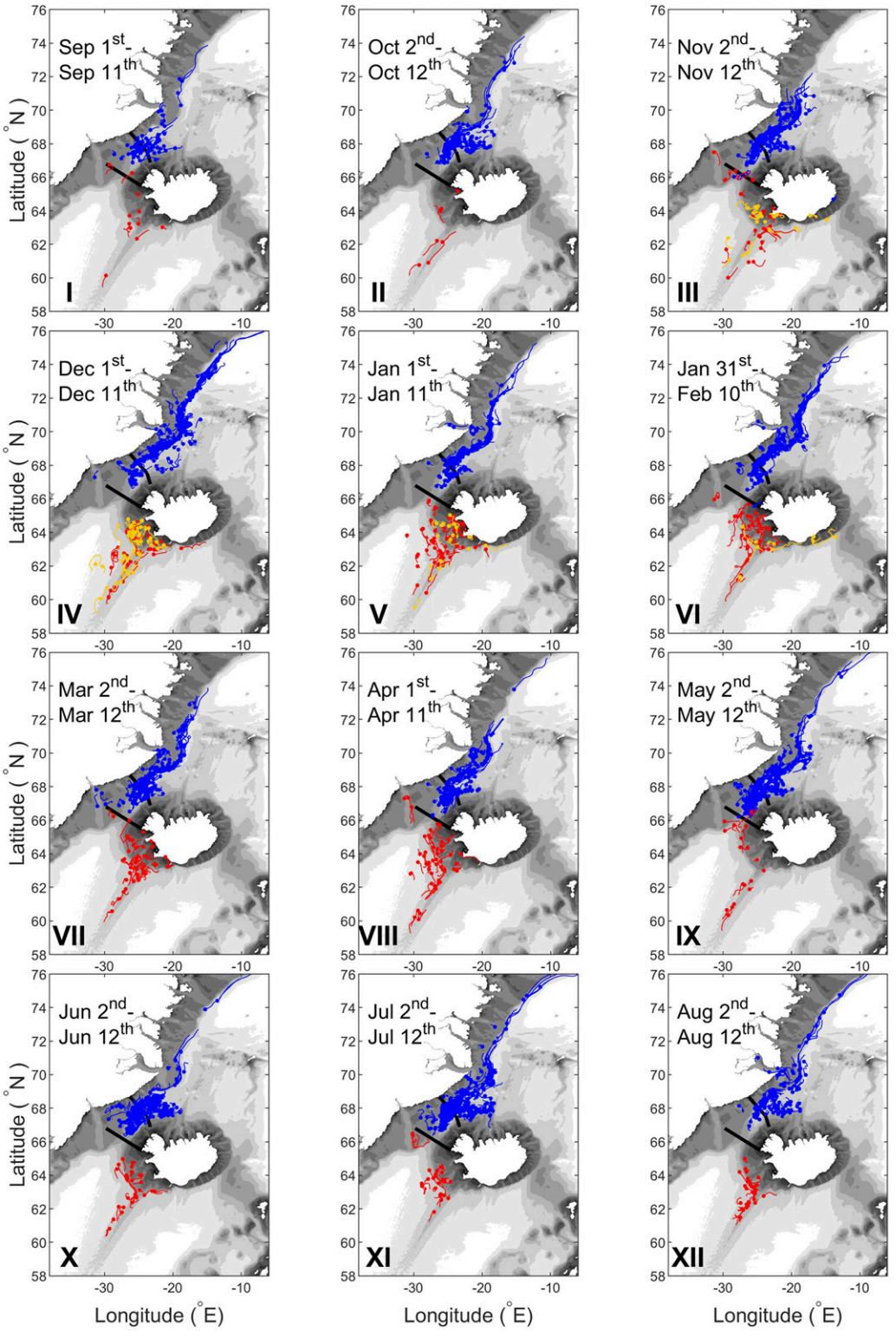

FIG. 8. The upstream trajectories of every 5th DSO particle in each subset moving toward the Látrabjarg section. Trajectories are plotted as pathline segments trailing behind particle markers for 10 days. The top date on each subplot shows the date at the origin (see also Table 2, column 3). The bottom date shows the date when particles are at their marker location. The faster the particles move, the longer are their tails. The particles are color coded by the origin subsets for each ensemble member as in Figs. 6b and 7 (see also the supplemental animation).

Downloaded from http://journals.ametsoc.org/jpo/article-pdf/50/8/2393/4989493/jpod190210.pdf by guest on 11 November 2020

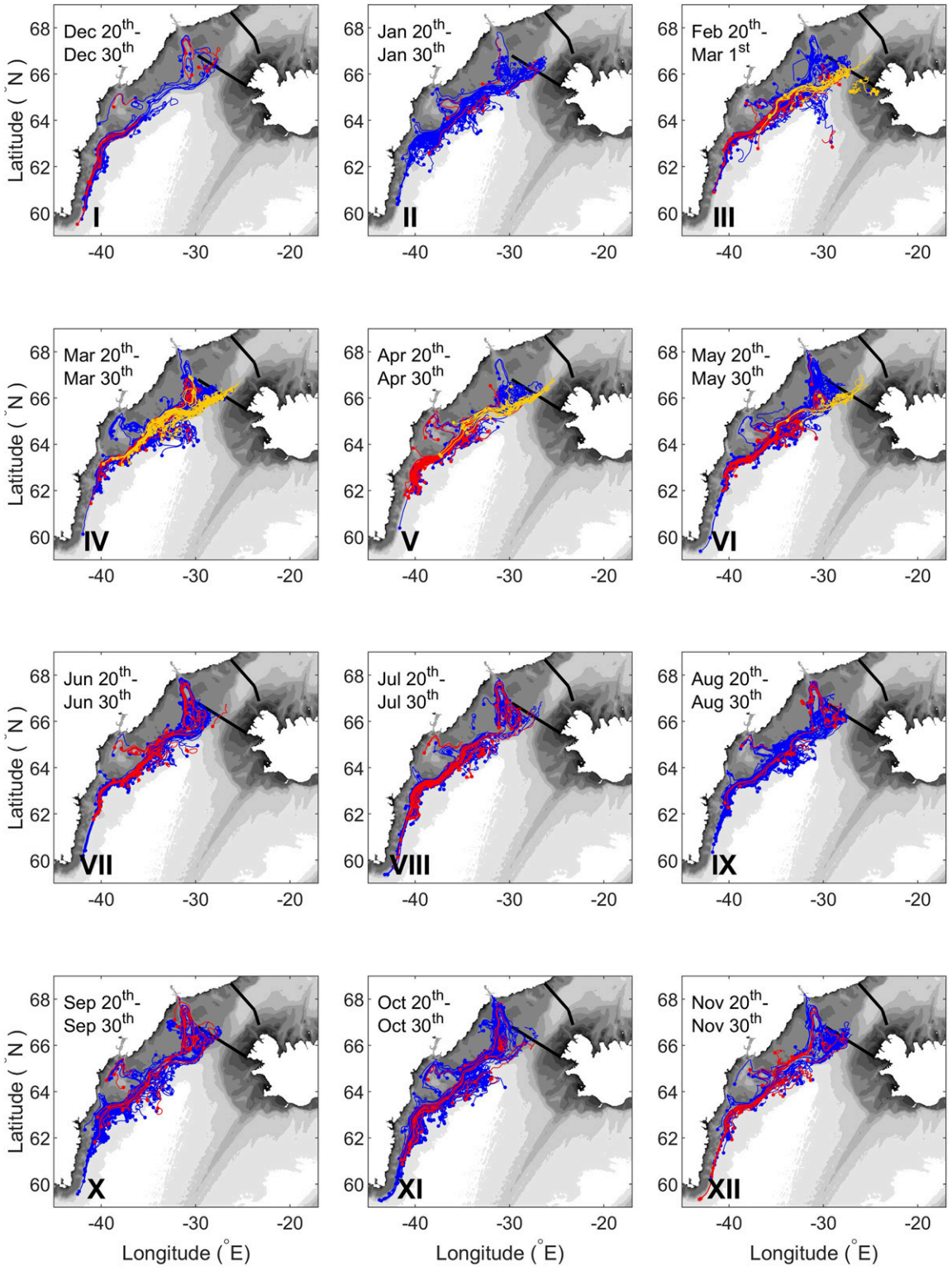

FIG. 9. As in Fig. 8, but after passing the Látrabjarg section.

Downloaded from http://journals.ametsoc.org/jpo/article-pdf/50/8/2393/4989493/jpod190210.pdf by guest on 11 November 2020

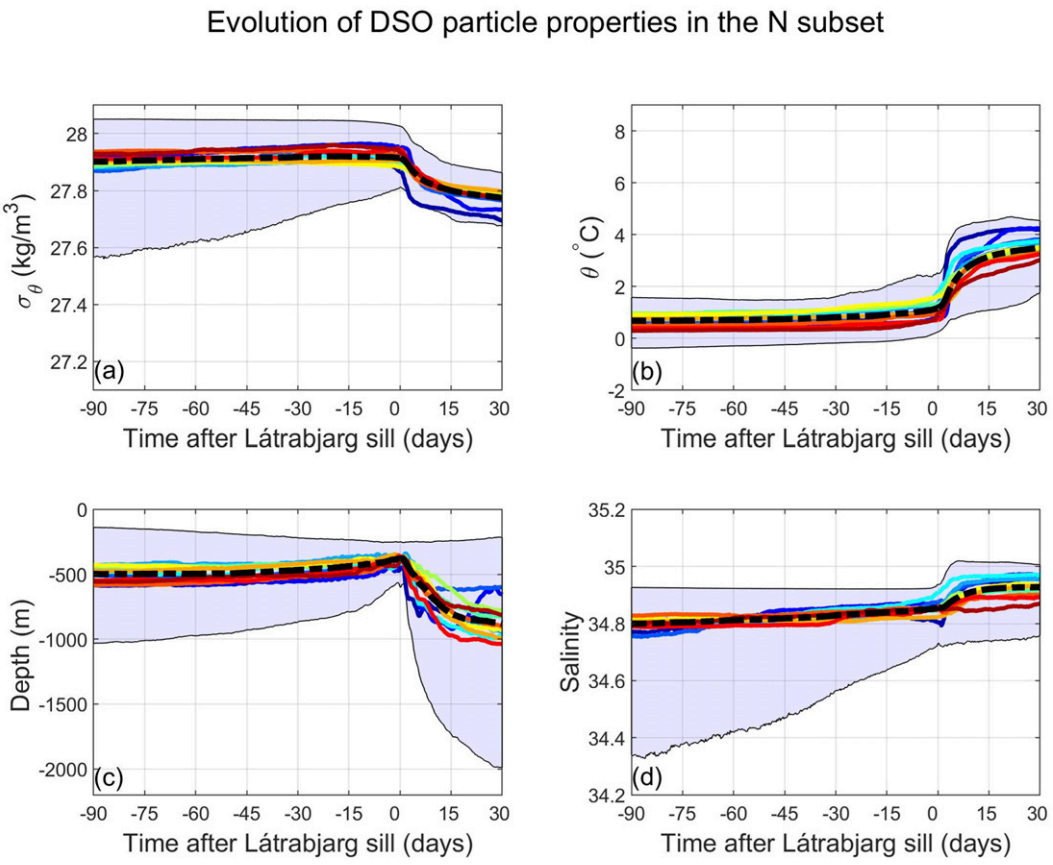

FIG. 10. The temporal evolution of (a) potential density, (b) potential temperature, (c) depth, and (d) salinity of the DSO particles in the N subset color coded by ensemble member (see Fig. 6a). The shading in each subplot marks the 5th and 95th percentiles of the DSO particle properties over all ensemble members. The individual colored solid lines show the mean properties for each ensemble member (consistent with the color codes in Fig. 6a). The black dash–dotted lines show the mean properties over all ensemble members. The abscissa shows the time line for the particles from the origin moving toward the Látrabjarg sill section (days 0) and after crossing it.

from all subsets follow nearly identical pathways. If the particles of each subset were not color coded differently, they would be indistinguishable. Here, the backward Lagrangian particle tracking elucidates the origins and trajectories of the DSO even in the regions of high mixing.

The evolution of hydrographic properties of DSO particles in the N, S, and ISh subsets are shown in Figs. 10–12, respectively. The mean temperature and salinity of the DSO particles in the N subset over all ensemble members (dash–dotted black lines) are nearly constant, with a slight increase ($\Delta\overline{T} = 0.4$°C, $\Delta\overline{S} = 0.05$) approaching the Denmark Strait sill (from −90 to 0 days). After cascading there is an increase in their temperature ($\Delta\overline{T} = 1.2$°C) and salinity ($\Delta\overline{S} = 0.1$) due to entrainment of the surrounding warmer and saltier water mass. The range of temperature before cascading is narrower (from −0.11° to 2°C) and it gets wider after cascading the Denmark Strait (from 1° to 4.5°C). The range of salinity however, is wider at the origin (34.3–34.9) and narrows approaching the Denmark Strait and after the cascade (34.7–35). The abrupt change is also evident in their potential density and depth. The DSO particles' mean potential density is nearly constant (less than 0.06 kg m^{-3} increase along the path) with the value of $\overline{\sigma_\theta} \approx 27.9$ kg m^{-3} from the origin until they reach the Denmark Strait. After cascading, their mean potential density decreases by about 0.15 kg m^{-3}. The depth of the DSO particles is also nearly constant approaching the Denmark Strait and they sink (900 m on average) as they cascade over the cataract. Notice that the DSO particles in ensemble members VI–IX are shallower than particles in ensemble members I–V at their origin and along their path to the Denmark Strait, but after cascading the DSO particles in all ensemble members experience similar initial deepening at least for the first 15 days (from approximately 360 to 1000 m).

The properties of the DSO particles in the S subset evolve differently (Fig. 11). Initially, the particle properties

Downloaded from http://journals.ametsoc.org/jpo/article-pdf/50/8/2393/4989493/jpod190210.pdf by guest on 11 November 2020

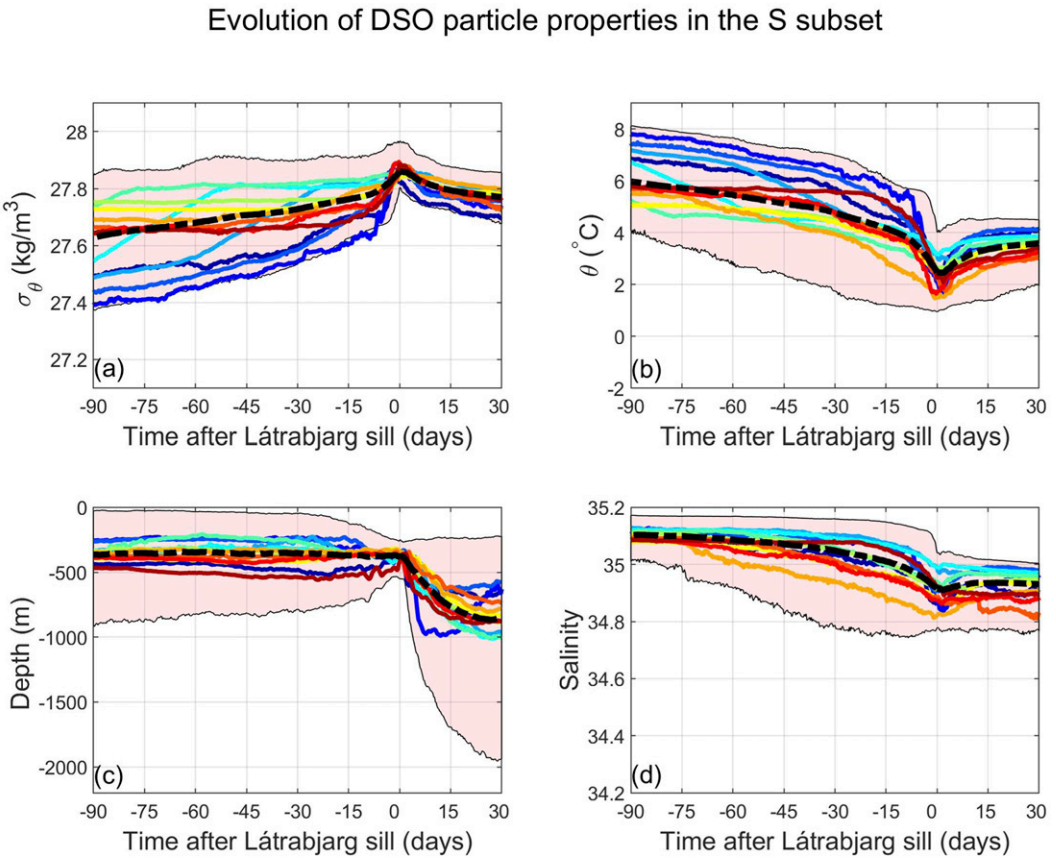

FIG. 11. As in Fig. 10, but for the DSO particles in the S subset.

are warmer and saltier than the DSO particles in the N subset at their origin location, but the S subset particles cool and freshen as they move toward the Denmark Strait. The rate of change of temperature is steeper for the I–V ($\Delta\overline{T} = -3.51$°C) than for the VI–XII ensemble members ($\Delta\overline{T} = -2.35$°C). The rate of change of salinity over all ensemble members is similar with an average of 0.15 decrease approaching the Denmark Strait from the origin. The DSO particles in the S subset are shallower and lighter at their origin in comparison to the DSO particles in the N subset but they rapidly densify while meeting the southward flowing DSO particles in the N subset (cf. Figs. 10a,c with Figs. 11a,c). After cascading, the DSO particles in the S subset have slightly higher average potential density ($0.08\,\mathrm{kg\,m^{-3}}$) than those in the N subset within the first 15 days after cascading. Ultimately, their properties become indistinguishable from the N subset. This is expected considering the intense mixing downstream of Denmark Strait shown earlier in Fig. 9.

The DSO particles in the ISh subset exist only in winter, for ensemble members III–VI (Fig. 12). They exhibit a similar cooling and freshening of their properties as the S subset, but the changes in their temperature happen at much faster rates. The cooling rate is more rapid for ensemble members III, IV, and V ($\Delta\overline{T} = -3.57$°C), and slower for ensemble member VI ($\Delta\overline{T} = -0.67$°C). The changes in the salinity are relatively small; the DSO particles in ensemble members III and IV slightly freshen ($\Delta\overline{S} = -0.03$) but those in ensemble members V and VI slightly salinify ($\Delta\overline{S} = 0.03$). The DSO particles in the ISh subset are generally shallower than the particles in the S subset (mean depth of 250 m) and they rapidly densify approaching the Denmark Strait. After crossing the sill (0 day) the DSO particles in the ISh subset still experience cooling, freshening and densification for approximately 15–20 days as opposed to the particles in the S subset. That is because the ISh subset particles still move northward along the shelf after crossing the Látrabjarg section and meet the southward flowing particles from the N subset, mix, and return south by cascading over the Denmark Strait within about 20 days of their forward run trajectories. Therefore, there is a lag in their property evolution with respect to the S and N subsets downstream of Denmark Strait.

To identify the water masses that the DSO particles carry, their distribution in potential temperature–salinity

Downloaded from http://journals.ametsoc.org/jpo/article-pdf/50/8/2393/4989493/jpod190210.pdf by guest on 11 November 2020

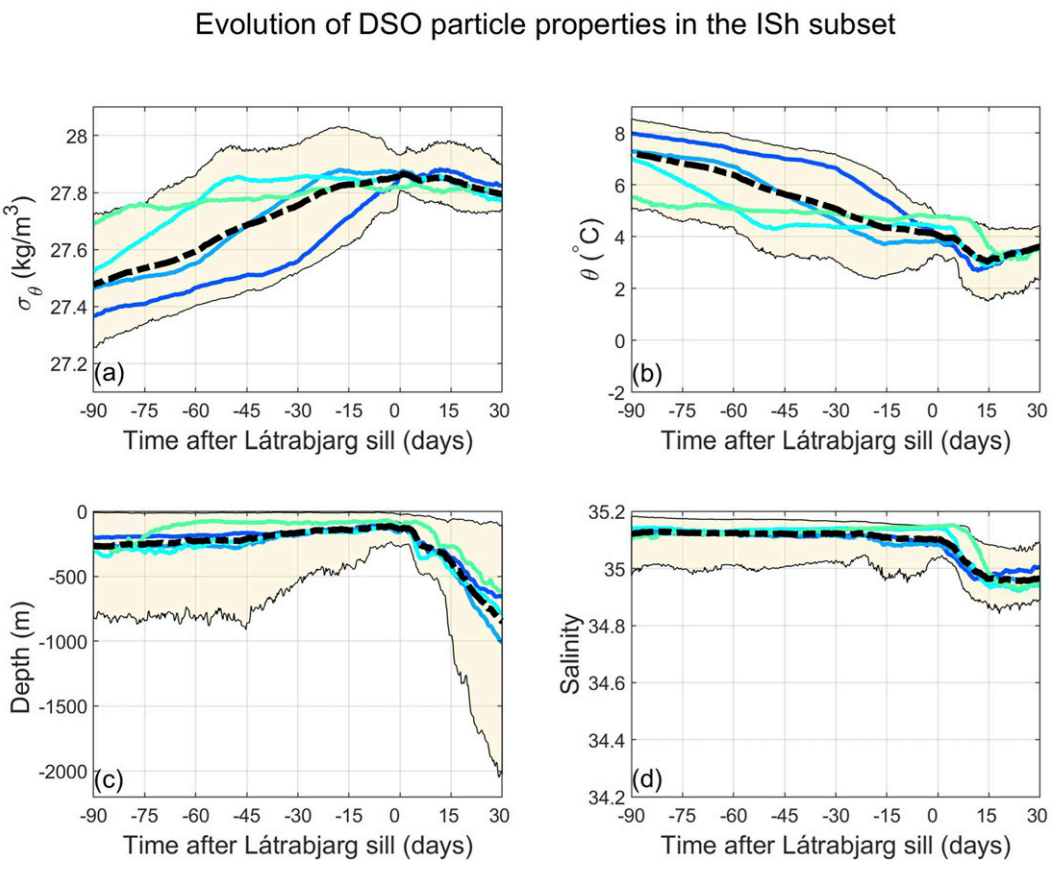

FIG. 12. As in Fig. 10, but for the DSO particles in the ISh subset. Note that the particles in this subset are only present in ensemble members III–VI.

(θ–S) space are plotted in Fig. 13 for all ensemble members, color coded based on their origins. The θ–S diagrams represent the water masses of the DSO particles at three different times: 1) at the origin, 2) at the release time at Látrabjarg, and 3) at the end point, 30 days after crossing the Denmark Strait. The DSO particles in the N subset at the origin (Fig. 13a) mark two hydrographic branches that indicate the conventional water mass end members observed north of Denmark Strait: the recirculated Atlantic Water, Polar Water, and Arctic Water (Harden et al. 2016). The particles in the ISh and S subsets contain the Irminger Water end member. These water masses are not distinguishable anymore at the Denmark Strait and farther downstream (Figs. 13b,c).

To identify when and where along the trajectories the water mass transformation takes place, the mean geographic location of the DSO particles in the latitude–longitude space as well as their mean trajectories in θ–S space are plotted (Fig. 14). The DSO particles in the N subset trace a short trajectory in θ–S space nearly along the 27.9 kg m^{-3} isopycnal from their origin to the Denmark Strait (Fig. 14b, blue). This indicates that the changes in their properties are small (Fig. 10a). However, their trajectory (in θ–S space) after cascading the Denmark Strait is longer, which means they have a larger and faster change of properties due to the mixing downstream of the Denmark Strait. The DSO particles' mean trajectory in the θ–S space crosses the 27.8 kg m^{-3} isopycnal and the DSO particles become lighter within 17 days after their cascade and continue to become more buoyant until the end of the simulation. As the N subset DSO particle trajectories are present both along the east Greenland shelf and west Iceland shelf, their mean geographic trajectories pass the middle of the Blosseville Basin, and after they cascade they continue along the east Greenland shelf.

The DSO particles in the S and ISh subsets behave differently (Fig. 14 red and yellow trajectories, respectively). The particles in the S subset cool and freshen along their trajectories from the origin to the Denmark Strait. They also densify until their potential density exceeds 27.8 kg m^{-3} approximately 9 days prior to reaching

Downloaded from http://journals.ametsoc.org/jpo/article-pdf/50/8/2393/4989493/jpod190210.pdf by guest on 11 November 2020

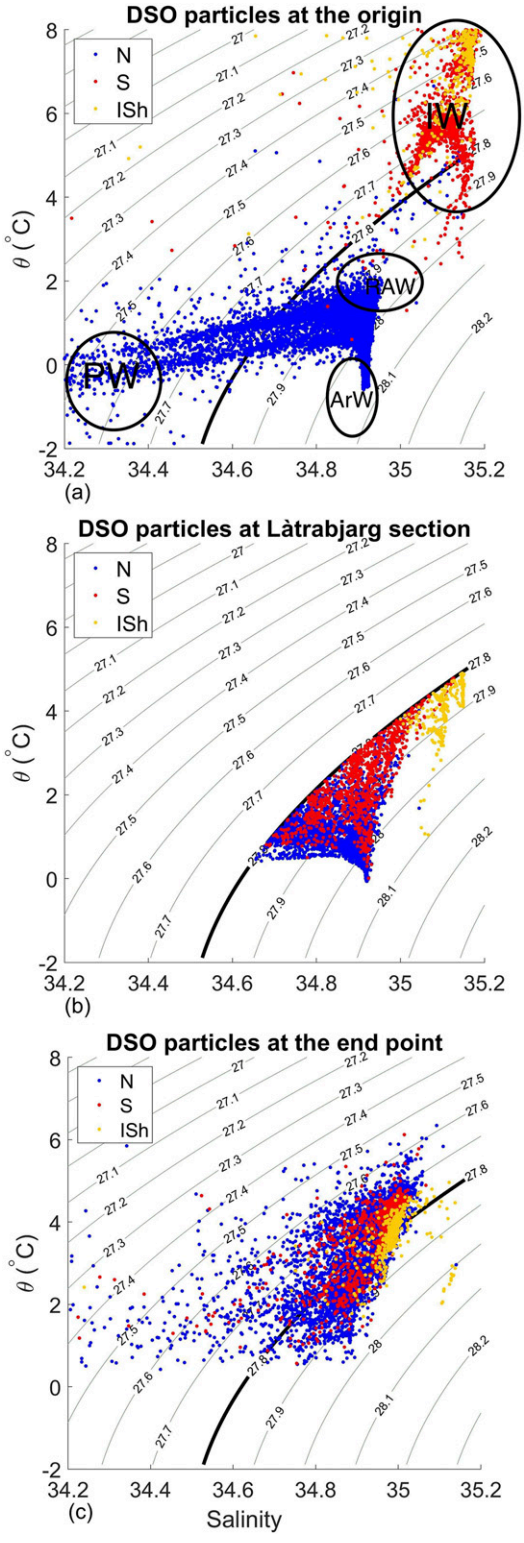

FIG. 13. Potential temperature–salinity (θ–S) diagrams for all of the DSO particles in all ensemble members at (a) the origin, (b) the Látrabjarg section, and (c) the end point, color coded by their origin. The water masses marked in panel (a) are Irminger Water (IW), Recirculated Atlantic Water (RAW), Arctic Water (ArW), and Polar Water (PW). The 27.8 kg m^{-3} isopycnal is highlighted by the bold black line.

the sill. Their trajectories in θ–S space from the origin to the Denmark Strait are quite long, which implies that they experience a faster rate of change in their properties than the N subset particles. After the cascade, they experience a shorter mean trajectory in θ–S space and become slightly lighter until their properties as well as their spatial location converges to that of the N subset DSO particles.

While moving along the Iceland shelf, the DSO particles in the ISh subset keep their salinity constant and cool until they are densified enough to cross the 27.8 kg m^{-3} isopycnal. This transformation takes place within 66 days of traveling from their origin to within about 50 km from the Denmark Strait. They still densify until they reach the Strait (green circle in Fig. 14). Then they continue along the 27.85 kg m^{-3} isopycnal for 24 days until they cross the Látrabjarg section while flowing northward along the Iceland shelf. They still continue moving north (in geographical space) and along the 27.85 kg m^{-3} isopycnal (in θ–S space). The mean trajectory continues along that isopycnal even after cascading for about 10 days. Finally, the mean trajectories of the ISh subset of DSO particles converge to that of the N and S subsets both in geographical and in θ–S space. This reflects the mixing downstream (cf. Figs. 9, 13b with Fig. 14). Note that the particles in the ISh subset, although starting as the shallowest, warmest and saltiest, become, after cascading, nearly as cold and fresh as the DSO particles in the N and S subsets.

4. Summary and conclusions

In this paper we presented a detailed analysis of upstream sources and pathways of the DSO. To do so, we performed a Lagrangian analysis on the output of a high-resolution ocean model to investigate the origins and pathways of the DSO. The model time period is from 1 September 2007 to 30 November 2008 and its outputs are evaluated by comparison with observations. This kinematic study gives a comprehensive understanding of the time-varying contribution to the overflow and evolution of previously identified northern pathways, i.e., the NIJ, the EGC, and the sEGC (blue curve in Fig. 6b). It also reveals an additional pathway from south of the Denmark Strait, which contributed to the DSO. This southern pathway itself is divided into two subsets, depending on whether the Lagrangian particles arrive at the sill east or west of 26.5°W. Those that arrive to the east of 26.5°W are shallower than 300 m and are present only during the winter. The average contribution from the south is 25.8% during the winter (JFM) of 2008, which has a relatively high NAO index. The entrainment south

Downloaded from http://journals.ametsoc.org/jpo/article-pdf/50/8/2393/4989493/jpod190210.pdf by guest on 11 November 2020

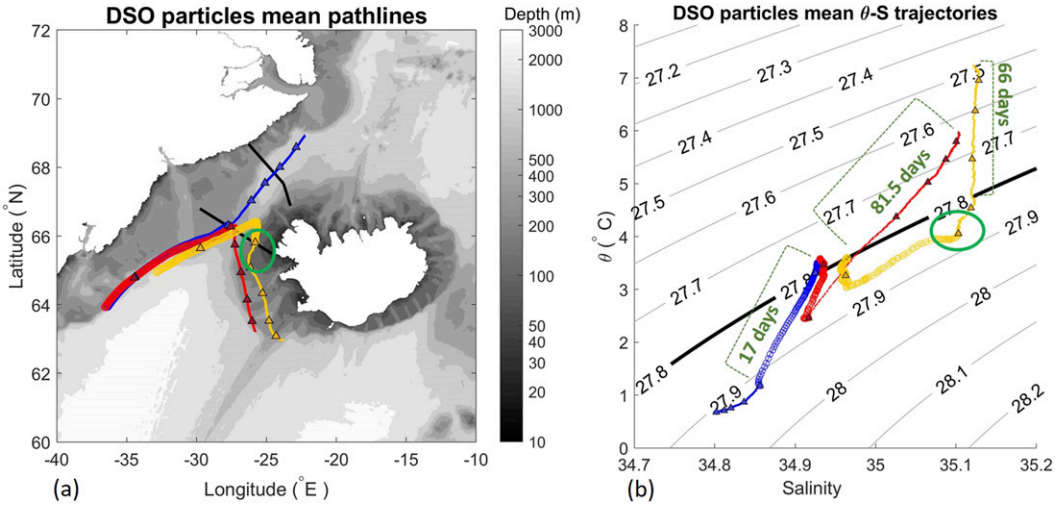

FIG. 14. The mean DSO particle trajectories in (a) geographical space and (b) θ–S space. The trajectories are color coded by their origins. The marker size is smaller for each trajectory from the origin to the Denmark Strait and it is bigger after crossing the Látrabjarg section. The trajectories are annotated with time, and every 20 days a triangle marker is added. The green circle marks the same timing both in geographical space and the θ–S space.

of Denmark Strait suggested by the literature, (e.g., cold entrainment of the northward Labrador Seawater (McCartney 1992), and warm entrainment of Irminger Current (von Appen et al. 2014) into the overflow at middepth and farther south of the sill) are different from the southern pathways we discovered. This subsurface southern pathway could potentially mark a shortcut for northward-flowing waters that densify and turn around to cascade over the Denmark Strait and eventually feeding the NADW. Although observations show evidence for the existence of the dense water on the Iceland shelf (Fig. 5; Våge et al. 2015) as well as presence of Irminger Water in the deep overflow (Mastropole et al. 2017), these southern pathways need more confirmation from observations. Future studies will benefit from models that incorporate coastal runoff on the Iceland shelf, and are several years long to account for interannual variability and to elucidate the relevance of these southern pathways in a changing climate.

The evolution of hydrographic properties of particles from each subset were also presented. The northern origin DSO particles (N subset) transform to become warmer, saltier and slightly less dense, but the southern origin DSO particles (S and ISh subsets) transform to become colder, fresher and denser along their path to the Denmark Strait. The DSO particle properties in all subsets converge after cascading over the Denmark Strait (Figs. 13b,c), and they have overlapping pathways (Fig. 9). Therefore, water mass analysis would not be able to discern the DSO sources at the Látrabjarg sill section or south of it. This study shows that the combination of backtracking and along-track water mass analysis can locate the water mass transformation sites continuously along the pathways (Fig. 14). In this way both time evolution and spatial distribution of pathways are required to determine the *origins* of the DSO water masses (see the introduction).

Finally, the schematic of the overflow water is updated by incorporating direct pathways of the DSO (Fig. 15). The circulation schematic shows that the separation from the EGC happens at multiple locations and it is intermittent. The DSO particles represent a clear distribution of pathways but they do not necessarily stay in one current (i.e., EGC, sEGC, and NIJ) at all times. Therefore, they do not indicate the currents, but rather trajectories of the particles. The particle pathways did not reveal an enduring source for the NIJ to the east of Kolbeinsey Ridge, but some particles show an intermittent eastern pathway (marked by dashed blue line in Fig. 15). The particle trajectories clearly marked the NIJ pathway from the north and west of Kolbeinsey Ridge toward Denmark Strait (e.g., Fig. 8, ensemble members II, IV, XI, and XII). This is similar to what was observed with the RAFOS floats (de Jong et al. 2018). We also see the core of the NIJ to the east of Kolbeinsey Ridge in the model mean Eulerian velocity field, consistent with Semper et al. (2019). Therefore, it is possible that an eastern source would be found if the Lagrangian simulation was multiyears long.

The southern pathways (revealed by the S and ISh subset particles) are the main addition to the previous schematics by Våge et al. (2013), Harden et al. (2016), and de Jong et al. (2018) although this contribution is likely to vary interannually depending on the local surface

Downloaded from http://journals.ametsoc.org/jpo/article-pdf/50/8/2393/4989493/jpod190210.pdf by guest on 11 November 2020

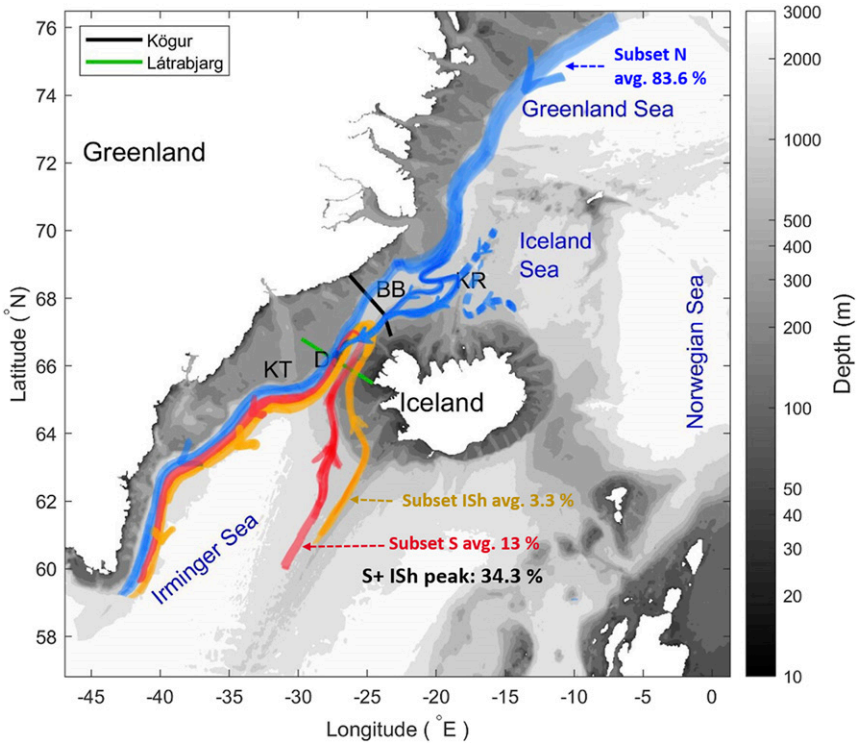

FIG. 15. The upstream and downstream schematic pathways of the DSO in the model. The annual average contribution (avg. %) from each subset and maximum contribution from the south (S + ISh) to the DSO origin are annotated.

forcing. These newly identified pathways (S + ISh) are shown to supply up to 34.3% of the DSO water, and is an important contribution to understanding the overflow water sources and composition. The highest contribution from the south is seen when there is more dense water on the Iceland shelf. The sparse in situ observational evidence suggests that there is a correlation between the existence of dense water ($\sigma_\theta \geq 27.8\,\mathrm{kg\,m^{-3}}$) on the shelf and a high winter NAO index, consistent with strong atmospheric cooling. However, the dynamical relationship between the atmospheric state and variability of dense water on the shelf needs more investigation and is left for future work. These dense water observations are mostly from the 1980s and 1990s when a warming trend of 0.2°–0.4°C decade^{-1} close to the bottom in the depth range of 100–250 m on the Iceland shelf was observed (Jochumsen et al. 2016). The warming can be another explanation for the missing dense profiles in recent years, in addition to the phase of the NAO. Determining the formation mechanism of the southern DSO sources is beyond the scope of this study, and could be a fruitful topic of future research.

Acknowledgments. This work was financially supported by the U.S. National Science Foundation under Grant Numbers OAC-1835640, OCE-1633124, OCE-1433448, and OCE-1259210. The authors thank Henrik Søiland, Institute of Marine Research, Bergen, Norway, for providing the CTD data at release time of RAFOS floats, and Benjamin E. Harden for providing the Kögur mooring array data. We thank Aleksi Nummelin, Mattia Almansi, and Soroosh Mani for providing constructive comments.

REFERENCES

Almansi, M., T. W. N. Haine, R. S. Pickart, M. G. Magaldi, R. Gelderloos, and D. Mastropole, 2017: High-frequency variability in the circulation and hydrography of the Denmark Strait Overflow from a high-resolution numerical model. *J. Phys. Oceanogr.*, **47**, 2999–3013, https://doi.org/10.1175/JPO-D-17-0129.1.

Bamber, J., M. van den Broeke, J. Ettema, J. Lenaerts, and E. Rignot, 2012: Recent large increases in freshwater fluxes from Greenland into the North Atlantic. *Geophys. Res. Lett.*, **39**, L19501, https://doi.org/10.1029/2012GL052552.

Behrendt, A., H. Sumata, B. Rabe, and U. Schauer, 2017: A comprehensive, quality-controlled and up-to-date data set of temperature and salinity data for the Arctic Mediterranean Sea (version 1.0), links to data files. PANGAEA, https://doi.org/10.1594/PANGAEA.872931.

Behrens, E., K. Våge, B. Harden, A. Biastoch, and C. W. Boning, 2017: Composition and variability of the Denmark Strait Overflow Water in a high-resolution numerical model hindcast

Downloaded from http://journals.ametsoc.org/jpo/article-pdf/50/8/2393/4989493/jpod190210.pdf by guest on 11 November 2020

simulation. *J. Geophys. Res. Oceans*, **122**, 2830–2846, https://doi.org/10.1002/2016JC012158.

Bromwich, D., and Coauthors, 2018: The Arctic System Reanalysis, version 2. *Bull. Amer. Meteor. Soc.*, **99**, 805–828, https://doi.org/10.1175/BAMS-D-16-0215.1.

Cooper, L., 1955: Deep water movements in the north Atlantic as a link between climatic changes around Iceland and biological productivity of the English channel and Celtic sea. *J. Mar. Res.*, **14**, 347–362.

Cummings, J. A., and O. M. Smedstad, 2014: Ocean data impacts in global HYCOM. *J. Atmos. Oceanic Technol.*, **31**, 1771–1791, https://doi.org/10.1175/JTECH-D-14-00011.1.

de Jong, M. F., H. Søiland, A. S. Bower, and H. H. Furey, 2018: The subsurface circulation of the Iceland Sea observed with RAFOS floats. *Deep-Sea Res. I*, **141**, 1–10, https://doi.org/10.1016/j.dsr.2018.07.008.

Dickson, R. R., and J. Brown, 1994: The production of north Atlantic deep water: Sources, rates, and pathways. *J. Geophys. Res.*, **99**, 12 319–12 341, https://doi.org/10.1029/94JC00530.

Donlon, C. J., M. Martin, J. Stark, J. Roberts-Jones, E. Fiedler, and W. Wimmer, 2012: The Operational Sea Surface Temperature and Sea Ice Analysis (OSTIA) system. *Remote Sens. Environ.*, **116**, 140–158, https://doi.org/10.1016/j.rse.2010.10.017.

Gelderloos, R., A. S. Szalay, T. N. Haine, and G. Lemson, 2016: A fast algorithm for neutrally-buoyant Lagrangian particles in numerical ocean modeling. *2016 IEEE 12th Int. Conf. on e-Science*, Los Alamitos, CA, IEEE Computer Society, 381–388, https://doi.org/10.1109/eScience.2016.7870923.

Haine, T., and Coauthors, 2008: North Atlantic deep water formation in the Labrador Sea, recirculation through the Subpolar Gyre, and discharge to the subtropics. *Arctic–Subarctic Ocean Fluxes: Defining the Role of the Northern Seas in Climate*, R. R. Dickson et al., Eds., Springer, 653–701, https://doi.org/10.1007/978-1-4020-6774-7_28.

Harden, B. E., and Coauthors, 2016: Upstream sources of the Denmark Strait Overflow: Observations from a high-resolution mooring array. *Deep-Sea Res. I*, **112**, 94–112, https://doi.org/10.1016/j.dsr.2016.02.007.

ICES, 2006: International council for the exploration of the seas hydrographic dataset. ICES, accessed 1 June 2019, https://doi.org/10.5065/D6X9291B.

Jackett, D. R., and T. J. McDougall, 1995: Minimal adjustment of hydrographic profiles to achieve static stability. *J. Atmos. Oceanic Technol.*, **12**, 381–389, https://doi.org/10.1175/1520-0426(1995)012<0381:MAOHPT>2.0.CO;2.

Jeansson, E., S. Jutterström, B. Rudels, L. G. Anderson, K. A. Olsson, E. P. Jones, W. M. Smethie, and J. H. Swift, 2008: Sources to the east Greenland current and its contribution to the Denmark Strait Overflow. *Prog. Oceanogr.*, **78**, 12–28, https://doi.org/10.1016/j.pocean.2007.08.031.

Jochumsen, K., S. M. Schnurr, and D. Quadfasel, 2016: Bottom temperature and salinity distribution and its variability around Iceland. *Deep-Sea Res. I*, **111**, 79–90, https://doi.org/10.1016/j.dsr.2016.02.009.

——, M. Moritz, N. Nunes, D. Quadfasel, K. M. H. Larsen, B. Hansen, H. Valdimarsson, and S. Jonsson, 2017: Revised transport estimates of the Denmark Strait Overflow. *J. Geophys. Res. Oceans*, **122**, 3434–3450, https://doi.org/10.1002/2017JC012803.

Jónsson, S., and H. Valdimarsson, 2004: A new path for the Denmark Strait Overflow water from the Iceland Sea to Denmark Strait. *Geophys. Res. Lett.*, **31**, L03305, https://doi.org/10.1029/2003GL019214.

Köhl, A., R. H. Käse, D. Stammer, and N. Serra, 2007: Causes of changes in the Denmark Strait Overflow. *J. Phys. Oceanogr.*, **37**, 1678–1696, https://doi.org/10.1175/JPO3080.1.

Koszalka, I. M., T. W. N. Haine, and M. G. Magaldi, 2013: Fates and travel times of Denmark Strait Overflow water in the Irminger Basin. *J. Phys. Oceanogr.*, **43**, 2611–2628, https://doi.org/10.1175/JPO-D-13-023.1.

——, T. W. Haine, and M. G. Magaldi, 2017: Mesoscale mixing of the Denmark Strait Overflow in the Irminger basin. *Ocean Modell.*, **112**, 90–98, https://doi.org/10.1016/j.ocemod.2017.03.001.

Lauvset, S. K., A. Brakstad, K. Våge, A. Olsen, E. Jeansson, and K. A. Mork, 2018: Continued warming, salinification and oxygenation of the Greenland sea gyre. *Tellus*, **70A**, 1–9, https://doi.org/10.1080/16000870.2018.1476434.

Legg, S., 2012: Tracer evidence of the origin and variability of Denmark Strait Overflow water. *Buoyancy-Driven Flows*, E. P. Chassignet, C. Cenedese, and J. Verron, Eds., Cambridge University Press, 203–239, https://doi.org/10.1017/CBO9780511920196.006.

Losch, M., D. Menemenlis, J. M. Campin, P. Heimbach, and C. Hill, 2010: On the formulation of sea-ice models. Part 1: Effects of different solver implementations and parameterizations. *Ocean Modell.*, **33**, 144–129, https://doi.org/10.1016/j.ocemod.2009.12.008.

Macrander, A., U. Send, H. Valdimarsson, S. Jónsson, and R. H. Käse, 2005: Interannual changes in the overflow from the Nordic seas into the Atlantic Ocean through Denmark Strait. *Geophys. Res. Lett.*, **32**, L06606, https://doi.org/10.1029/2004GL021463.

——, R. Käse, U. Send, H. Valdimarsson, and S. Jónsson, 2007: Spatial and temporal structure of the Denmark Strait Overflow revealed by acoustic observations. *Ocean Dyn.*, **57**, 75–89, https://doi.org/10.1007/s10236-007-0101-x.

Malmberg, S.-A., and H. Valdimarsson, 2003: Hydrographic conditions in Icelandic waters, 1990-1999. *ICES Mar. Sci. Symp.*, **219**, 50–60.

Marshall, J., A. Adcroft, C. Hill, L. Perelman, and C. Heisey, 1997: A finite-volume, incompressible Navier-Stokes model for studies of the ocean on parallel computers. *J. Geophys. Res.*, **102**, 5753–5766, https://doi.org/10.1029/96JC02775.

Mastropole, D., R. S. Pickart, H. Valdimarsson, K. Våge, K. Jochumsen, and J. Girton, 2017: On the hydrography of Denmark Strait. *J. Geophys. Res. Oceans*, **122**, 306–321, https://doi.org/10.1002/2016JC012007.

Mauritzen, C., 1996: Production of dense overflow waters feeding the North Atlantic across the Greenland-Scotland Ridge. Part 1: Evidence for a revised circulation scheme. *Deep-Sea Res. I*, **43**, 769–806, https://doi.org/10.1016/0967-0637(96)00037-4.

McCartney, M., 1992: Recirculating components to the deep boundary current of the northern North Atlantic. *Prog. Oceanogr.*, **29**, 283–383, https://doi.org/10.1016/0079-6611(92)90006-L.

Moritz, M., K. Jochumsen, R. P. North, D. Quadfasel, and H. Valdimarsson, 2019: Mesoscale eddies observed at the Denmark Strait sill. *J. Geophys. Res. Oceans*, **124**, 7947–7961, https://doi.org/10.1029/2019JC015273.

NOAA, 2013: World Ocean Database. NOAA, https://www.nodc.noaa.gov/OC5/SELECT/dbsearch/dbsearch.html.

Noël, B., W. J. van de Berg, H. Machguth, S. Lhermitte, I. Howat, X. Fettweis, and M. R. van den Broeke, 2016: A daily, 1 km resolution data set of downscaled Greenland ice sheet surface mass balance (1958–2015). *Cryosphere*, **10**, 2361–2377, https://doi.org/10.5194/tc-10-2361-2016.

Downloaded from http://journals.ametsoc.org/jpo/article-pdf/50/8/2393/4989493/jpod190210.pdf by guest on 11 November 2020

North, R. P., K. Jochumsen, and M. Moritz, 2018: Entrainment and energy transfer variability along the descending path of the Denmark Strait Overflow plume. *J. Geophys. Res. Oceans*, **123**, 2795–2807, https://doi.org/10.1002/2018JC013821.

Østerhus, S., and Coauthors, 2019: Arctic Mediterranean exchanges: A consistent volume budget and trends in transports from two decades of observations. *Ocean Sci.*, **15**, 379–399, https://doi.org/10.5194/os-15-379-2019.

Palsson, J., O. S. Astthorsson, and H. Valdimarsson, 2012: Hydrographic variability in Icelandic waters during recent decades and related changes in distribution of some fish species. *ICES J. Mar. Sci.*, **69**, 816–825, https://doi.org/10.1093/icesjms/fss027.

Pickart, R. S., and Coauthors, 2017: The North Icelandic jet and its relationship to the north Icelandic Irminger current. *J. Mar. Res.*, **75**, 605–639, https://doi.org/10.1357/002224017822109505.

Pratt, L. J., and J. A. Whitehead, 2008: *Rotating Hydraulics*. Springer, 589 pp., https://doi.org/10.1007/978-0-387-49572-9.

Price, J. F., and M. O. Baringer, 1994: Outflows and deep water production by marginal seas. *Prog. Oceanogr.*, **33**, 161–200, https://doi.org/10.1016/0079-6611(94)90027-2.

Rossby, T., D. Dorson, and J. Fontaine, 1986: The RAFOS system. *J. Atmos. Oceanic Technol.*, **3**, 672–679, https://doi.org/10.1175/1520-0426(1986)003<0672:TRS>2.0.CO;2.

Rudels, B., P. Eriksson, E. Fahrbach, G. Budéus, and J. Meincke, 2002: The East Greenland current and its contribution to the Denmark Strait Overflow. *ICES J. Mar. Sci.*, **59**, 1133–1154, https://doi.org/10.1006/jmsc.2002.1284.

Sakov, P., F. Counillon, L. Bertino, K. A. Lisæter, P. R. Oke, and A. Korablev, 2012: TOPAZ4: An ocean-sea ice data assimilation system for the north Atlantic and Arctic. *Ocean Sci.*, **8**, 633–656, https://doi.org/10.5194/os-8-633-2012.

Semper, S., K. Våge, R. S. Pickart, H. Valdimarsson, D. J. Torres, and S. Jónsson, 2019: The emergence of the north Icelandic jet and its evolution from northeast Iceland to Denmark strait. *J. Phys. Oceanogr.*, **49**, 2499–2521, https://doi.org/10.1175/JPO-D-19-0088.1.

Smethie, W. M., Jr., and J. H. Swift, 1989: The tritium:krypton-85 age of Denmark Strait Overflow Water and Gibbs Fracture Zone Water just south of Denmark strait. *J. Geophys. Res.*, **94**, 8265–8275, https://doi.org/10.1029/JC094iC06p08265.

Spall, M. A., R. S. Pickart, P. Lin, W.-J. von Appen, D. Mastropole, H. Valdimarsson, T. W. N. Haine, and M. Almansi, 2019: Frontogenesis and variability in Denmark Strait and its influence on overflow water. *J. Phys. Oceanogr.*, **49**, 1889–1904, https://doi.org/10.1175/JPO-D-19-0053.1.

Swift, J. H., and K. Aagaard, 1981: Seasonal transitions and water mass formation in the Iceland and Greenland Seas. *Deep-Sea Res.*, **28A**, 1107–1129, https://doi.org/10.1016/0198-0149(81)90050-9.

——, ——, and S.-A. Malmberg, 1980: The contribution of the Denmark Strait Overflow to the deep North Atlantic. *Deep-Sea Res.*, **27A**, 29–42, https://doi.org/10.1016/0198-0149(80)90070-9.

Tanhua, T., K. Bulsiewicz, and M. Rhein, 2005a: Spreading of overflow water from the Greenland to the Labrador Sea. *Geophys. Res. Lett.*, **32**, L10605, https://doi.org/10.1029/2005GL022700.

——, K. A. Olsson, and E. Jeansson, 2005b: Formation of Denmark Strait Overflow water and its hydro-chemical composition. *J. Mar. Syst.*, **57**, 264–288, https://doi.org/10.1016/j.jmarsys.2005.05.003.

——, ——, and ——, 2008: Tracer evidence of the origin and variability of Denmark Strait Overflow water. *Arctic–Subarctic Ocean Fluxes*, R. R. Dickson, J. Meincke, and P. Rhines, Eds., Springer, 475–503. https://doi.org/10.1007/978-1-4020-6774-7_21.

Våge, K., R. S. Pickart, M. A. Spall, H. Valdimarsson, S. Jónsson, D. J. Torres, S. Østerhus, and T. Eldevik, 2011: Significant role of the North Icelandic jet in the formation of Denmark Strait Overflow water. *Nat. Geosci.*, **4**, 723–727, https://doi.org/10.1038/ngeo1234.

——, ——, ——, G. Moore, H. Valdimarsson, D. J. Torres, S. Y. Erofeeva, and J. E. O. Nilsen, 2013: Revised circulation scheme north of the Denmark Strait. *Deep-Sea Res. I*, **79**, 20–39, https://doi.org/10.1016/j.dsr.2013.05.007.

——, G. Moore, S. Jónsson, and H. Valdimarsson, 2015: Water mass transformation in the Iceland Sea. *Deep-Sea Res. I*, **101**, 98–109, https://doi.org/10.1016/j.dsr.2015.04.001.

Valdimarsson, H., and S. Malmberg, 1999: Near-surface circulation in the Icelandic waters derived from satellite tracked drifters. *Rit Fiskideildar*, **16**, 23–39.

von Appen, W.-J., and Coauthors, 2014: The East Greenland spill jet as an important component of the Atlantic meridional overturning circulation. *Deep-Sea Res. I*, **92**, 75–84, https://doi.org/10.1016/j.dsr.2014.06.002.

Downloaded from http://journals.ametsoc.org/jpo/article-pdf/50/8/2393/4989493/jpod190210.pdf by guest on 11 November 2020